
# Residence times of groundwater along a flow path in the Great Artesian Basin determined by 81Kr, 36Cl and 4He: Implications for palaeo hydrogeology

R. Purtschert, A.J. Love, W. Jiang, Z.-T. Lu, G.-M. Yang, S. Fulton, D. Wohling, P. Shand, W. Aeschbach-Hertig, L. Broder, P. Müller, Y. Tosaki

PII: S0048-9697(22)06986-8

DOI: https://doi.org/10.1016/j.scitotenv.2022.159886

Reference: STOTEN 159886

To appear in: *Science of the Total Environment*

Received date: 23 August 2022

Revised date: 28 October 2022

Accepted date: 28 October 2022

Please cite this article as: R. Purtschert, A.J. Love, W. Jiang, et al., Residence times of groundwater along a flow path in the Great Artesian Basin determined by 81Kr, 36Cl and 4He: Implications for palaeo hydrogeology, *Science of the Total Environment* (2022), https://doi.org/10.1016/j.scitotenv.2022.159886

# Residence times of groundwater along a flow path in the Great Artesian Basin determined by $^{81}Kr$, $^{36}Cl$ and $^{4}He$: Implications for palaeo hydrogeology

R. Purtschert[1,£], A.J. Love[2], W. Jiang[3], Z-T. Lu[3], G-M. Yang[3], S. Fulton[4], D. Wohling[5], P.Shand[2], W. Aeschbach-Hertig[6], L. Broder[6*], P. Müller[7], Y. Tosaki[8],

[1]Climate and Environmental Physics, University of Bern, Switzerland

[2]College of Science and Engineering and the NCGRT, Flinders University, Adelaide, Australia

[3]University of Science and Technology of China, Hefei, China.

[4]Fulton Independent Consultant Australia

[5]Innovative Groundwater Solutions, Wayville, Australia,

[6]Institute of Environmental Physics, Heidelberg University, Germany

[7] ATTA Laboratory, Argonne National Laboratory, USA

[8]Geological Survey of Japan, AIST, Tsukuba, Ibaraki 305-8567, Japan

[*]now at Dept. of Earth Science, ETH Zurich, Switzerland

[£]corresponding author: Roland Purtschert (roland.purtschert@unibe.ch)

# Abstract

Understanding the age distribution of groundwater can provide information on both the recharge history as well as the geochemical evolution of groundwater flow systems. Of the few candidates available that can be used to date old groundwater, $^{81}$Kr shows the most promise because its input function is constant through time and there are less sources and sinks to complicate the dating procedure in comparison to traditional tracers such as $^{36}$Cl and $^{4}$He. In this paper we use $^{81}$Kr in a large groundwater basin to obtain a better understanding of the residence time distribution of an unconfined-confined aquifer system. A suite of environmental tracers along a groundwater flow path in the south–west Great Artesian Basin of Australia have been sampled. All age tracers ($^{85}$Kr, $^{39}$Ar $^{14}$C, $^{81}$Kr, $^{36}$Cl and $^{4}$He) display a consistent increase in groundwater age with distance from the recharge area indicating the presence of a connected flow path. Assuming that $^{81}$Kr is the most accurate dating technique the $^{36}$Cl/Cl systematics was unravelled to reveal information on recharge mechanism and chloride concentration at the time of recharge. Current-day recharge occurs via ephemeral river recharge beneath the Finke River, while diffuse recharge is minor in the young groundwaters. Towards the end of the transect the influence of ephemeral recharge is less while diffuse recharge and the initial chloride concentration at recharge were higher.



## 1 Introduction

The Great Artesian Basin (GAB) is a continental-scale multi-layered aquifer system, one of the largest groundwater basins in the world (Habermehl, 1980). Because of its large size and relatively easy access to free-flowing artesian waters it has been considered an ideal “field laboratory” for the application and assessment of dating old groundwater. Previous investigations have included seminal studies on Chlorine-36 ($^{36}$Cl) (Bentley et al., 1986a; Torgersen et al., 1991), Helium-4 ($^{4}$He) (Torgersen and Clarke, 1985) and in more recent times Krypton-81 ($^{81}$Kr) (Collon et al., 2000; Lehmann et al., 2003). In the latter study accelerator mass spectrometry (AMS) measurements of the $^{81}$Kr abundancies were

conducted for the first time in a regional study of the same part of the GAB as presented here. Of these three isotopes, $^{81}$Kr is the most suitable for age interpretation of old groundwater, because $^{36}$Cl and $^{4}$He are often not straightforward to untangle as they are complicated by uncertain model assumptions. Along a hydraulic transect from the Finke River recharge zone in the south-western GAB (Figure 1), we constrained groundwater flow velocities by a set of dating tracers that cover time ranges from decades ($^{85}$Kr) to over hundreds and thousands of years ($^{39}$Ar, $^{14}$C), and to hundreds of thousands of years ($^{81}$Kr,$^{36}$Cl).

The most used tracer for dating very old groundwater is $^{36}$Cl (half-life 301 kyr). The widespread availability of Accelerator Mass Spectrometry (AMS) from the late 1980s meant that $^{36}$Cl could henceforth not only be sampled easily but analysed relatively routinely. This combined with the high solubility of chloride resulted in widespread optimism in the research community that the ultimate methodology for dating old groundwater was within reach. However, this optimism soon faded when it was realised that much more complementary information would be required to interpret $^{36}$Cl, including the spatial and temporal variability of the $^{36}$Cl input as well as information about sources and sinks of chloride. The reader is referred to a number of comprehensive reviews on $^{36}$Cl (Aggarwal et al., 2013; Phillips, 2000). In this paper we demonstrate that with independent knowledge of the groundwater age chronology from $^{81}$Kr measurements, we have the potential to unravel the chlorine isotope systematics and the chloride input into the groundwater system. This procedure provides additional information on the groundwater flow system not possible by other methodologies, and under ideal situations it may provide “proxy” evidence for paleoclimate.

Helium-4 is another isotope commonly used to obtain information on old groundwater (Kipfer et al., 2002). The basic principle of this method is that, as $^{4}$He is produced in the sub surface by the decay of uranium (U) and thorium (Th) its concentration increases with increasing residence time. For quantitative age dating the local accumulation rate of $^{4}$He needs to be determined as well as the He influx to the aquifer from various sources. The production rate can be calculated from U and Th concentrations in the aquifer. However, the

He influx from neighbouring strata is far more difficult to quantify. As a result, $^{4}$He is often considered to be a semi-quantitative indicator of groundwater age at best. Many previous studies in the GAB have been devoted to the accumulation of He in groundwater (Torgersen and Clarke, 1985, 1987; Torgersen and Ivey, 1985). However, up until the present, it has not been possible for the $^{4}$He clock to be calibrated against a reliable residence time indicator, not only for the GAB, but also for other large aquifers systems around the globe (Torgersen, 2010)

It is only recently that the detection of $^{81}$Kr at natural levels has been developed with a precision sufficient to date groundwater (Gerber et al., 2017; Jiang et al., 2020; Matsumoto et al., 2018; Ram et al., 2021; Sturchio et al., 2014; Yechieli et al., 2019; Yokochi et al., 2019; Yokochi et al., 2021), but it has for a long time been potentially considered to be the most reliable isotope to quantify long groundwater residence times (Lehmann et al., 1993; Lehmann et al., 2003). This is because krypton (Kr), being a noble gas is inert and as a result does not undergo chemical reactions. Furthermore, it has a well-known atmospheric concentration of 1.099 ± 0.009 ppm (Aoki and Makide, 2005). Variations of the $^{81}$Kr/Kr ratio over time are relatively small (Buizert et al., 2013; Zappala et al., 2020). In addition, both subsurface and anthropogenic sources of $^{81}$Kr are considered minimal in most cases (Aggarwal et al., 2015; Purtschert et al., 2013; Purtschert et al., 2021; Sturchio et al., 2004). However the application of this potentially ideal groundwater tracer has been limited in the past because of poor detection efficiency of $^{81}$Kr which has resulted in large volumes of water required for degassing (Purtschert et al., 2013). Nevertheless, recent development of Atom Trap Trace Analysis method (ATTA) has improved the detection efficiency, which has resulted in a much lower volume of water being required for sampling and processing (Lu et al., 2014; Zappala et al., 2020; Zhang et al., 2020).

Our study area is in the south -western GAB. This region may represent an ideal area for testing the application of $^{81}$Kr in groundwater studies because: a) the hydrogeology of the region is relatively well known (Love et al., 2013); b) there have been previous studies on the source and sinks of chloride (Love et al., 2000); c) there have been numerous hydro-chemical and environmental tracers studies in the region (Priestley et al., 2017; Radke et al., 2000;

Herczeg et al., 1988) and, d) the first successful set of groundwater $^{81}Kr$ samples were analysed by AMS in this region (Collon et al., 2000; Lehmann et al., 2003). It is assumed that there has been effectively zero diffuse recharge in the region since the end of the Pleistocene and that modern day recharge only occurs beneath isolated riverbeds referred to as ephemeral river recharge (ERR) (Fulton et al., 2013).

In this paper we show that $^{81}Kr$ ages provide a reasonable representation of the groundwater residence time. Our confidence in this comes from the lack of major sources or sinks of Kr in the subsurface and that the input function is known and constant through time. Furthermore, a previous study in this area, provided the first $^{81}Kr$ dates from four wells in the region, indicating that this new dating tool was worthy of further consideration (Lehmann et al 2003).

The aim of this paper is to:

- Assess the feasibility of radioactive noble gas tracers ($^{85}Kr$, $^{81}Kr$ and $^{39}Ar$) for the determination of groundwater flow velocities over a large range of flow distances.
- Use the calculated $^{81}Kr$ ages to calibrate the $^{36}Cl$ and $^{4}He$ groundwater clocks.
- Obtain a better understanding of the paleo hydrogeology and in particularly the history of recharge from the Finke River over time.

## 2 Study area

Our study area is the western margin of the GAB in the Finke River recharge zone and extents hundreds of kilometres towards the interior of the GAB where the aquifer becomes confined (Figure 1). The study section starts near the Finke River recharge zone and extends about 300 km downstream. At the beginning of the transect the main aquifer of the GAB (referred to as the Cadna-Owie Formation–Algebuckina Sandstone or J aquifer in this section of the GAB) crops out and is unconfined for approximately 40 km until it becomes a confined system overlain by the confining Bulldog Shale. The study area is arid with potential evapotranspiration ranging up to 3000 mm/yr. Average annual rainfall is 200 mm/yr, with approximately 85 % occurring in the months of January to March. In this area of the GAB the only effective recharge occurring today is via ephemeral river recharge (ERR). This recharge

to the main J aquifer of the GAB occurs in the outcrop area beneath the Finke River where the main J aquifer outcrops during infrequent times of intense rainfall that originate from monsoons that travel across the continent from the north. Stable isotope data indicate that this typically occurs in the months of January to March (Fulton et al 2013).

Fulton et al. (2013) mapped the potential recharge zone to be 13 $km^2$, with a length of 36 km and an average river bed width of 370 m. (Fulton et al 2013). Ephemeral river recharge beneath the Finke River recharge zone was estimated to be 380-850 mm per annum, in contrast to diffuse recharge surrounding the river which is in the order 0.1-0.25 mm/yr. (Wohling et al., 2013). Groundwater flows in a southeast direction from the Finke River recharge zone to towards a more central portion of the GAB. Clearly, modern day ERR occurs beneath the Finke River today but how significant this recharge has been in the past remains unresolved

Previous studies in the arid central Australia have shown that subsurface production of $^{36}Cl$, as well as diffusion of solutes from adjacent aquitards, complicates the interpretation of $^{36}Cl$ dating results (Love et al., 2000; Priestley et al., 2017). Furthermore, it has been shown that there are spatial variations in the $^{36}Cl/Cl$ input value, and in all cases, the input values are below what could be expected from latitudinal variation of the $^{36}Cl/Cl$ input ratio alone. Based on Cl/Br in samples upstream from the Finke River recharge zone halite dissolution has occurred from the Bitter Springs Formation and has been discharged to the river. This effect can account for the lower $^{36}Cl/Cl$ input value of 60 x $10^{-15}$ (Fulton et al., 2013; Wohling et al., 2013). While in the region to the south–west of the Finke River recharge zone there is no evidence of young groundwater being influenced by dissolution of evaporates. In this area the $^{36}Cl/Cl$ input ratio was determined to be 125 x$10^{-15}$ based on measurements on selected young groundwater samples in the unconfined part of this aquifer where an anthropogenic component can be ruled out (Lehmann et al., 2003; Love et al., 2000).

# 3 Field and Analytical Methods

Groundwater was sampled from unconfined and confined sections (including artesian wells) of the main J aquifer of the GAB (Figure 1). The sampling sites were selected along a transect in the direction of groundwater flow. The transect begins in the Finke River recharge area and extends past Dalhousie Springs. A total of 19 wells were purged several times until stable field parameters of pH, temperature and salinity were achieved (Table 1).

Samples for $^{4}$He were taken in copper tubes using standard techniques (Aeschbach-Hertig and Solomon, 2013). He isotopes, as well as the main isotopes of Ne and the heavy noble gases were measured at the Institute of Environmental Physics, Heidelberg University, following the methods described by (Beyerle et al., 2000). Radioactive noble gases $^{85}$Kr, $^{39}$Ar and $^{81}$Kr were sampled in the field using a large volume gas extraction system (Purtschert et al., 2013). The vacuum cylinder gas extraction system was optimized for remote fieldwork and achieved an extraction efficiency of 80-90% at a water flow rate of 20 L/min. Approximately 2000-3000 L of groundwater were degassed in the field and gases were collected in pre-evacuated steel containers.

The gas obtained by degassing was analysed for major gas composition on a quadrupole mass spectrometer before separating the Ar and Kr gases for further analysis. Krypton was extracted from the bulk gas at the University of Bern by multistep gas chromatography (Loosli and Purtschert, 2005), and the isotope ratios $^{81}$Kr/Kr and $^{85}$Kr/Kr were determined using the ATTA-3 instrument in the Laboratory for Radiokrypton Dating, Argonne National Laboratory (Jiang et al., 2012). Based on the Atom Trap Trace Analysis method (Du et al., 2003), ATTA-3 is a selective and efficient atom counter capable of measuring both $^{81}$Kr/Kr and $^{85}$Kr/Kr ratios of environmental samples in the range of $10^{-14}$ – $10^{-10}$. In the apparatus, atoms of a targeted isotope ($^{81}$Kr, $^{85}$Kr, or the control isotope $^{83}$Kr) were captured by resonant laser light into an atom trap and counted by observing the fluorescence of the trapped atoms. For $^{81}$Kr dating in the age range of 50 kyr – 1,500 kyr, the required sample size was at the time of analyses 5 – 10 micro-L STP of krypton gas, which could be extracted from approximately 100 – 200 kg of water or 40 – 80 kg of ice. Both the reliability and reproducibility of the method were examined with an inter-comparison study among

different methods and instruments. The $^{85}Kr/Kr$ ratios of 12 samples, in the range of $10^{-13}$ to $10^{-10}$, were measured independently in three laboratories: a low-level counting (LLC) laboratory in Bern, Switzerland, and two ATTA laboratories, one in Argonne and the other in Hefei, China. The results agree at the precision level of 7% (Du et al., 2003; Jiang et al., 2012).

The detection limit of ATTA-3, defined as the lowest isotope ratio detectable by ATTA-3, is approximately 1 dpm/cc for $^{85}Kr/Kr$. Here we use the conventional units of dpm/cc, which stands for the number of $^{85}Kr$ decays per minute per mL-STP of Kr gas. For conversion, 100 dpm/cc corresponds to the $^{85}Kr/Kr$ ratio of $3.03 \times 10^{-11}$. This detection limit, caused by the instrument memory effect, was determined with measurements of an $^{85}Kr$-dead sample. Argon was also extracted from the bulk gas by cryogenic distillation. $^{39}Ar$ activities were measured by low-level gas proportional counting at the Physics Institute, University of Bern (Loosli, 1983; Loosli and Purtschert, 2005).

Radiocarbon ($^{14}C$) was collected in 1 litre bottles in the field and analysed by AMS at the Rafter Radiocarbon Laboratory in New Zealand. An additional aliquot collected for Carbon 13 ($^{13}C$) was also analysed at the same laboratory. $^{36}Cl$ samples were filtered with 0.45 µm membrane filters and then the chloride was prepared as AgCl according to the preparation scheme reported in (Tosaki et al., 2011). The $^{36}Cl/Cl$ ratios were analysed with the AMS (accelerator mass spectrometry) system at the Tandem Accelerator Complex, University of Tsukuba (Sasa et al., 2010), along with diluted NIST $^{36}Cl$ standards ($^{36}Cl/Cl = 1.60 \times 10^{-12}$).

# 4 Results

For ease of comparison and discussion the sampled wells were split into three groups (Figure 1):

- Group I samples located closest to the Finke River recharge zone (red dots in figures)
- Group II represent the intermediate wells (green triangles in figures)
- Group III represent the wells furthest along the transect (blue triangles in figures)

Well 19 is an outlier and does not belong to any group. The groundwater there most likely originates from a westerly recharge source (black square in figures).

## *4.1 Radionuclides data consistency and reduction*

The purpose of this section is to review the internal consistency of the data set and to apply corrections to the data where required. The activities of the radioactive noble gases $^{85}$Kr, $^{39}$Ar, $^{81}$Kr as well as $^{14}$C activities and $^{36}$Cl/Cl ratios are summarized in Table 2, and tracer-tracer plots are compared with each other in order of increasing half-lives in in Figure 2.

Figure 2a displays three samples with elevated $^{85}$Kr values in combination with $^{39}$Ar values < 20% of the activity in the modern atmosphere (pmAr). These are possibly the result of contamination of the Kr gas fraction which was purified and shipped to Argonne National Laboratory after the Ar gas fraction was separated at the University of Bern from the crude gas which implies that only the $^{81}$Kr activities need to be corrected (and not $^{39}$Ar). This is the case for samples 9 and 14. The $^{81}$Kr value of the highly air contaminated sample 7 was neglected**.** Since it is assumed that the contamination occurred in the northern hemisphere the corresponding atmospheric $^{85}$Kr activity in the norther hemisphere ($^{85}Kr_{atm}$) of 75 dmp/cc Kr (Winger et al., 2005) was used to calculate the fraction $\alpha$ of air contamination in the $^{81}$Kr sample ($\alpha = {}^{85}Kr_m/{}^{85}Kr_{atm}$).

$$^{81}Kr_{corr} = \frac{(^{81}Kr_m - \alpha \cdot 100)}{1-\alpha} \qquad \text{Eq 1}$$

Here the indices *m* and *corr* refer to the measured and corrected $^{81}$Kr values, respectively. $^{81}$Kr activity is given in percent of the modern atmospheric value (pmKr).

The comparison of $^{39}$Ar and $^{14}$C activities reveals a rather consistent pattern (Figure 2b). The $^{39}$Ar active samples show the highest $^{14}$C activities ranging from 40-90 pmC (percent modern carbon). Three samples from Group 1 and all samples from Group 2-3 have $^{39}$Ar activities (given in percent of the modern atmospheric activity concentration pmAr) below the detection limit except for sample 12 which has an elevated $^{39}$Ar value. Since this sample is $^{85}$Kr free, air contamination during sampling can be excluded. The $^{39}$Ar activity was measured

twice with reproducible results so we are confident that the value is real. One possibility could be that this sampling location represents modern recharge from vertical flow from the surface. However, this seems very unlikely as this location is a zone of upward hydraulic head which would negate downward flow today. This site also has 320 m of overlying low permeability units. Furthermore, all the other dating tracers indicate old groundwater. Locally elevated underground in-situ production of $^{39}$Ar within in the aquifer at great depth (Lehmann et al., 1993) cannot be excluded but seems to be unlikely because the $^{39}$Ar values of all others samples from Groups 2-3 are below detection limit in agreement with previous findings (Lehmann et al., 2003). However, this site also has elevated $^{36}$Cl/Cl in comparison to the depleted $^{81}$Kr value (**Error! Reference source not found.**d). This may possibly support the existence of a locally elevated neutron flux (Purtschert et al., 2021). We interpret this as a local phenomenon and assume negligible underground production of $^{39}$Ar for all other samples. The $^{39}$Ar values of Group 1 were therefore interpreted in terms of groundwater residence time without corrections for underground production.

Elevated $^{14}$C activities of Group 1 waters coincide with the highest $^{81}$Kr values (Figure 2c). Samples with $^{81}$Kr values <80 % modern are strongly depleted in $^{14}$C with values between 3-10 pmc. However, even the most $^{81}$Kr depleted waters have $^{14}$C concentrations significantly above the detection limit of ~0.5 pmC. The origin of this offset of ~4 pmC remains a conundrum but may be an analytical artefact rather than representing the real situation in the aquifer. $^{14}$C contamination e.g. during sampling was observed in other studies (Aggarwal et al., 2014; Yokochi et al., 2017) in particular when conventional sampling and counting techniques were applied. Such an effect was however not expected for the radiocarbon AMS technique as applied in our study. The comparison with the $^{81}$Kr data in combination with the improbability of the admixture of young water components in the downstream part of the artesian aquifer allows us to conclude that samples with $^{14}$C activities below 4 pmc are older than the practical upper end of the $^{14}$C dating range of 40 kyrs.

$^{81}$Kr activities and $^{36}$Cl/Cl ratios correlate well (**Error! Reference source not found.**d). The largest scatter is observed for Group 1 where $^{36}$Cl/Cl ratios range between 40-90 x $10^{-15}$ for a relatively small range of $^{81}$Kr values between 80 and 100 %modern. Further downstream

(Groups 2-3) the activities of both tracers decrease simultaneously. A more detailed discussion of both tracers in terms of groundwater residence time and flow velocity will follow in section 5.1.

$\delta^{13}C$ values of DIC (Table 1) are relatively constant along the flow line and range mostly between -10 to -12‰. This is comparable to the assumed signature of soil $CO_2$ (Fulton et al., 2013). This indicates that dissolution of carbonate minerals during recharge beneath the Finke River is minimal. As a result, we present $^{14}C$ ages (Table 2) calculated with a constant initial activity of 86 pmC calculated from the mean of $^{39}Ar$ active samples under consideration of an offset of 4 pmC (section 5.1).

## *4.2 Spatial distribution of tracer activities*

In Figure 3 the contamination corrected tracer activities are plotted as a function of distance from the recharge area (RA), where the Finke River crosses the J aquifer outcrop.

$^{85}Kr$ values (Table 2, not shown in the graph) below 2.4 dpm/ccKr indicate a lower age limit of 40 years for all waters. This is also supported by the highest $^{39}Ar$ activity of 65 ±7 pmAr which corresponds to a residence time of ~170 years. With increasing distance from the recharge area, the $^{39}Ar$ values decreases rapidly to the below detection limit around 40 km from the Finke River. This is also the location where a sharp decrease of $^{14}C$ activities is observed. Within 10-20 km, the $^{14}C$ activities decreases from 70 to 17 pmC (Figure 3c). This rapid decrease in $^{14}C$ corresponds to the approximate location where the aquifer transfers from an unconfined to a confined system (Figure 1). In this section the aquifer thickness increases from 30 m to almost 200 m which may imply a reduction of the flow velocity.

All Group 1 waters show modern or slightly sub-modern $^{81}Kr$ activities (Figure 3d). For Group 2 groundwater wells the $^{14}C$ ages increase beyond the dating range of the radiocarbon method. This is consistent with the decreasing $^{81}Kr$ activities in this area (**Error! Reference source not found.**d and 3e). The lowest $^{81}Kr$ values of 34 and 36 pmKr are observed for Group 3 groundwaters. This corresponds to an $^{81}Kr$ age of ~ 350 kyrs. Sample number 13 appears to be closely related to Sample 19 being sourced from the west (Figure 1). It has a

higher $^{81}$Kr value than would be expected if it were along a common flow transect from the north. Figure 3e shows that the highest $^{36}$Cl/Cl ratios are found close to the recharge area. Most samples of Group 1 cluster at $^{36}$Cl/Cl ratios in the range 50-60 x $10^{-15}$. Similarly to $^{81}$Kr, the ratios decrease within Group 2 and reach the lowest values in Group 3 wells down gradient. Although there is considerably more scatter in the $^{36}$Cl/Cl values.

Concentrations of dissolved $^{4}$He also show a very pronounced evolution with distance (Figure 3f). Group 1 water close to the recharge area are low in $^{4}$He with concentrations < $10^{-6}$ $cm^3_{STP}/g_w$. Within Group 2 an increase is observed after approximately 150 km from the Finke River recharge area. Waters of Group 3 are most enriched in $^{4}$He by three orders of magnitude in relation to air saturated water (ASW). Also here sample 13 is an outlier with a lower $^{4}$He concentration suggesting a shorter flow path from a westerly source as indicated by the potentiometric surface (Figure 1, note no $^{4}$He data are available for sample 19).

## *4.3 Stable isotopes*

The stable isotope composition of the groundwater varies over a large range between -10.7 ‰ to -6 ‰ for $\delta^{18}O$ and -74 ‰ to -43 ‰ and for $\delta^{2}H$ (Table 1 and **Error! Reference source not found.**). The most depleted waters are from Group 1 close to the recharge area. Further downgradient (Group 2 & 3), the stable isotope composition is characterised by more enriched values. The best fit of the data has a slope of is 6.4±0.2, while the deuterium excess (defined by $\delta^{2}H - 8x\delta^{18}O$) decreases from +11‰ in the recharge area to +3.5‰ for the oldest waters. This indicates that groundwater that infiltrated in the past was subject to greater evaporation than the younger waters. This is also supported by the highest Cl concentrations found for Group 2 and Group 3 waters. However, it must be considered that part of the chlorine accumulated in the subsurface. This distinction is made in the discussion, taking into account the $^{81}$Kr ages.

# 5 Discussion

## 5.1 Groundwater residence times and flow velocities

The comprehensive set of dating tracers covering age ranges of decades ($^{85}$Kr) to centuries ($^{39}$Ar) to millennia's ($^{14}$C) and up to hundreds of thousands of years ($^{81}$Kr, $^{36}$Cl and $^{4}$He) along a groundwater flow path consistently indicate increasing residence time with decreasing piezometric heads and distance from the Finke River recharge area (Table 2). This unique dataset allows for the inter-comparison of the suitability of the different dating tracers, particular in relation to $^{81}$Kr data, and for an understanding of the recharge and flow dynamic of this part of the GAB. The very old apparent residence times imply recharge over different climate periods.

In this paper, the term "tracer age" refers to the decay (or accumulation in the case of $^{4}$He) time of the individual tracer that has been elapsed between groundwater recharge and the sampling location in the aquifer system. The distinct half-lives (and decay constants $\lambda$) of $^{39}$Ar, $^{14}$C and $^{81}$Kr cover very different ranges of residence times, *t*. The $^{39}$Ar, $^{14}$C and $^{81}$Kr percent modern values are converted directly to groundwater ages using the radioactive decay law: .

$$t = \frac{1}{\lambda} \cdot \ln\left(\frac{C_0}{C}\right) \qquad \text{Eq 2}$$

where C and $C_0$ are the measured and initial concentration respectively. For $^{39}$Ar and $^{81}$Kr, initial activities $C_0$ of 100 pmAr and 100 pmKr were assumed. An initial $^{14}$C concentration of 86 pmC was calculated from the mean of samples with a detectable $^{39}$Ar activity (samples 2, 3 and 8 in Figure 8). From this initial value and from all measured activities an offset of 4 pmC was subtracted as outlined in section 4.1. The resulting tracer ages for $^{39}$Ar, $^{14}$C and $^{81}$Kr are listed in Table 2 and are compared in Figure 5 with age bands considering the analytical uncertainties. The Figure demonstrates consistent tracer ages for most wells without consideration of mixing, but it becomes also obvious how the application of tracers with suitable half-life reduces the age uncertainties for the individual age ranges.

A fit through the decay ages of sampling points reveal the mean flow velocity between those sampling points, which is independent of the initial concentration $C_0$ (Figure 6). Thereby it is assumed that the observed gradient of tracer concentrations along a flow line is mainly the result of aging rather than mixing of different water masses (i.e. piston flow). The age gradients are determined individually for $^{39}Ar$, $^{14}C$ and $^{81}Kr$ (Figure 6 A, B and C). For $^{14}C$, two different slopes were calculated for the first part of the transect and the further downstream part, respectively.**Error! Reference source not found.** The fitting results are depicted in Figure 6 and show a clear trend as function of flow distance, time and dating tracer. On short timescales and as calculated from the $^{39}Ar$ data a flow velocity of ~90 m/yr close to the recharge can be derived. Downstream, the $^{14}C$ data indicate a further decrease of the flow velocity to ~10.9 m/yr up to ~ 30 kms, while further downgradient (~ 30 -90 kms) flow velocities decrease to ~4 m/yr. A similar pattern for the $^{81}Kr$ data can be observed where, on $^{81}Kr$ timescales of hundreds of thousands of years an average flow velocity of ~ 1 m/yr can be concluded. Further downgradient (~150-300 kms) these deceases to ~0.3 m/yr (Figure 6). Figure 6D, displays the various calculated velocities from the different tracers versus an analytical model of tracer velocity (see Section 6.2). The decrease of flow velocities (or increase of spatial age gradients) as function of flow and tracer timescales may have several reasons:

- The assumption of conservative flow within the aquifer is not fulfilled. If significant quantities of water seep through the aquitards (leaky aquitards) the flow velocity within the aquifer would decrease according to the mass conservation law. The observed reduction of flow velocity along the flow line by two orders of magnitude would imply that 99% of the recharge is lost by upward leaking through the aquitard.
- Transient hydrodynamic conditions either due to naturally changing recharge rates and/or the change from pre-exploitation conditions to a situation with heavy groundwater abstraction would modify the age gradient within the system. A new tracer steady state in the whole system is only achieved after a transient phase during which the new hydraulic state propagates through the system (Rousseau-Gueutin et al., 2013; Zuber et al., 2010). However, if the mean groundwater age is

large in comparison with the characteristic timescale of the changes in the system, as it is the case here, a hydrologic quasi-steady state can still be assumed.

- Also, the progressive admixture of older water along the flow line would cause a faster aging along the flow than anticipated in a piston flow scenario. Towards the centre of the basin the reginal flow directions from the western and the north-eastern recharge areas converge (Radke and Sciences, 2000; Torgersen et al., 1991)) which could cause an apparent spatial aging.
- Dominant recharge at a point source, as it is postulated in our study area today, into a 3-dimensional aquifer system would also lead to a decreasing flow velocity as function of distance from the source.

We judge the last possibility to be the most likely and this scenario is investigated in more detail in the following section.

## *5.2 Finke River recharge source*

One of the key questions that remains unresolved in understanding ephemeral river recharge (ERR) in this part of the GAB is how long the Finke River has been a source of groundwater recharge. For the following analyses we hypothesize that the Finke River recharge zone is a point source. This seems reasonable considering that the section where the Finke River crossed the outcrops of the J-aquifer is only 36 km long and 350 m in width which is relatively small considering a transect distance of more than 300 km. Then, if we assume steady state groundwater flow in an aquifer with constant porosity and recharge from a point source with strength S ($m^3$/yr) and the law of mass conservation it follows that:

$$S = v_D(R) \cdot A(R) \qquad \text{Eq. 3}$$

Where $v_D(R)$ is the Darcy velocity and $A(R)$ the cross section where groundwater moves as function of distance R from the point source (Figure 7). The cross-sectional area $A(R)$ may increase because of radial flow away from the point source (which is strictly not fulfilled) it follows from Eq.3 that the local Darcy velocity, $v_D(R)$, decreases inversely proportional with distance R from the point source: $v_D(R) \sim \frac{1}{R}$. For constant porosity $\phi$, this relationship is

also valid for the water flow velocity $v=v_D/\phi$. Then, the total flow time T to a certain distance R from the point source is:

$$T(R) \sim \int_0^R \frac{1}{v(R')} dR' \sim \int_0^R R'\, dR' \sim R^2 \qquad \text{Eq. 4}$$

implying that $R(T) \sim T^{0.5}$. Consequently, the flow velocity decreases as function of residence time T according to:

$$v(T) = \frac{dR(T)}{dT} \sim T^{-n} \quad \text{Eq. 5}$$

with n=0.5. In a three-dimensional case (where H is also increasing with distance) n would be 0.66. The analytical model above is plotted against the observed tracer velocity data in Figure 6D. We note that this distribution follows one that we would expect from a point source and conclude that our data are consistent with the presence of the actual Finke River recharge plume (Radke and Sciences, 2000). Whether ERR was also the dominating recharge mechanism in the past or for group 2-3 waters cannot be concluded from the dating tracers alone. For this purpose, methods and tracers that are sensitive to recharge mechanisms are required.

## 5.3 Systematics of $^{36}Cl$ and Cl

If we accept that $^{81}Kr$ provides the most accurate chronology of old groundwater residence times of up to 400,000 years between the Finke River and Dalhousie Springs, we can then try to evaluate the temporal evolution of $^{36}Cl$ (expressed as the $^{36}Cl/Cl$ and Cl concentration) as well as the different source of chloride. The chloride mass balance as function of groundwater residence time can generally be expressed as (Bentley et al., 1986b; Phillips, 2000).

$$\underset{a}{R \cdot C} = \underbrace{R_i \cdot C_i \cdot \exp(-\lambda_{36} \cdot t)}_{b} + \underbrace{R_{Se} \cdot C_i \cdot (1 - \exp(-\lambda_{36} \cdot t))}_{c} + \underbrace{(C - C_i) \cdot R_{Ex}}_{d} \qquad \text{Eq. 6}$$

where,

**a**: Measured $^{36}Cl$ concentration in the sample (atoms/L water) expressed as the product of $^{36}Cl/Cl$ ratio R and chloride concentration C

**b**: Decay of the initial $^{36}Cl$ concentration in recharge water, which is defined by the $^{36}Cl/Cl$ ratio at recharge ($R_i$) and the initial chloride concentration $C_i$

**c**: In-growth of a secular subsurface equilibrium $^{36}Cl$ concentration within the aquifer, which is given by the equilibrium ratio $R_{SE}$ and the initial concentration $C_i$

**d**: $^{36}Cl$ accumulation due to the addition of Cl from subsurface sources ($C_a=C-C_i$) with a $^{36}Cl/Cl$ ratio from the external source of $R_{Ex.}$

If Cl behaves physically and chemically conservative (no sources or sinks of Cl within the aquifer) only the term **b** must be considered. However, even in this simple case, assumptions must be made about the local $^{36}Cl/Cl$ initial ratio $R_i$ which could vary spatially and temporally. Neutron activation of the dissolved $^{35}Cl$ by the reaction $^{35}Cl(n,\gamma)^{36}Cl$ would continuously add $^{36}Cl$ atoms until a secular production decay equilibrium $R_{se}$ is reached, as described by term **c**. It is thereby again assumed that the Cl concentration in the water is constant over time. $R_{Se}$ can be estimated based on the elemental composition of the aquifer rocks (Lehmann et al., 1993). However, in the investigated part of the GAB the assumption of constant Cl concentration is not fulfilled (Figure 9). The Cl concentration increases quasi-linearly with groundwater residence time at an apparent growth rate of ~3.1 mg/L/kyr (Figure 9). This increase can either be because of Cl accumulation from subsurface sources (Love et al., 2000) and/or due to changes of the initial chloride concentration $C_i$ as a result of varying evaporative enrichment at recharge time..

Without additional information from other tracers, it is impossible to separate both **b** and **c** processes (and $^{36}Cl$ dating is not possible in this case). However, our $^{81}Kr$ data now offer the unique opportunity to better constrain the Cl accumulation history and to deconvolute the relative importance of both processes as a function of groundwater flow time and distance. This information is not only crucial for the characterization of the accumulation processes along the flow path but also for the reconstruction of past recharge conditions which affect

the evaporative enrichment of $C_i$. This in turn, provides information about the dominant recharge mechanism as function of time i.e., the importance of ERR versus diffusive recharge. For this purpose, the initial $^{36}Cl$ and Cl concentration of the different recharge sources need to be defined.

## *5.4 Initial parameters*

The initial $^{36}Cl/Cl$ at recharge must be estimated based on recent samples which infiltrated prior to 1950 to exclude the contribution of bomb derived $^{36}Cl$ to estimate groundwater residence times of old groundwater. Previous estimates (Love et al., 2000) concluded an average initial $R_i$ in precipitation and groundwater of 125±10 x $10^{-15}$~ 600 km to the south-west of our study area. In this area, the dominant recharge mechanism is diffuse.

The best candidates in our study area are $^{85}Kr$ free samples (thus free of $^{36}Cl$ from the nuclear tests in the 1960's) with detectable $^{39}Ar$ and $^{14}C$ activities (therefore containing fresh recharge on the $^{36}Cl$ timescale). Almost all samples of Group 1 fulfil these criteria (Figure 8). The highest $^{36}Cl/Cl$ ratio was measured at site 3 with a value of 91 ± 5 x $10^{-15}$. However, most samples with young $^{39}Ar$ and $^{14}C$ signatures have a much lower $^{36}Cl/Cl$ ratio around 55-60 x $10^{-15}$ (Figure 3 and 8). Considering the half-lives of $^{36}Cl$ (310 kyr), $^{39}Ar$ (269 yr) and $^{14}C$ (5730 yr), $^{36}Cl$ decay can be excluded as the reason for the $^{36}Cl/Cl$ depletion of those samples compared to sample 3 or samples found elsewhere in this part of the GAB (Love et al., 2000 and Figure 7). The admixture of old groundwater is also unlikely because Group 1 water are located close to the outcrop and presumed recharge area of the J aquifer and because the quasi modern $^{81}Kr$ activities do not indicate the presence of a substantial old water component (Figure 3 and Figure 6).

The only reasonable explanation is that the source of recharge is not direct precipitation, but water with a low $^{36}Cl/Cl$ due to the addition of chloride with a depleted $^{36}Cl$ signature. Indeed, water sampled along the Finke River (New Crown Station and Old Crown Town) showed $^{36}Cl/Cl$ of 60 x $10^{-15}$ and 64 x $10^{-15}$, respectively (Fulton et al., 2013). The depleted $^{36}Cl/Cl$ ratio

of the Finke River, compared to local precipitation, originates from halide dissolution e.g. from the Bitter Springs Formation which crops out along the Finke River further upstream (Fulton et al., 2013). That way ERR from the Finke River is tagged with an initial ratio $R_{ERR}$= ($60\times10^{-15}$) and a relatively low Cl concentration of ~100 mg/L ($C_i$). Significantly higher initial concentrations are likely due to a different recharge process, with initial ratio $^{36}Cl/Cl$ ratio ($R_D$) and chloride concentration ($C_D$). Confirming the finding of the previous dating section, this indicates that ERR dominates under present climate conditions with an initial $^{36}Cl/Cl$ ratio $R_i$ of 60 x $10^{-15}$ as indicated by the mean of Group 1 samples (Figure 2 and Figure 8). The average Cl concentration of Group 1 is ~ 100-200 mg/L which most likely represents the initial concentration $C_i$ for ERR ($C_{ERR}$ in Eq. 8). Since ERR is a relatively rapid recharge mechanism, it is unlikely that the higher Cl concentrations found further down the groundwater flow path are caused by changes of $C_{ERR}$ in the past. The Cl increase of Group 2 and Group 3 samples further downstream may have two reasons: (i) temporal variations of environmental conditions triggering a different recharge mechanism that leads to higher Cl concentrations at recharge, or (ii) accumulation of Cl originating from subsurface sources.

In case of a more humid climate in the past, diffusive recharge over large surface areas would dominate and the initial $R_i$ would have been closer to the typical value of local precipitation (120-130 x $10^{-15}$). This would also imply higher Cl concentrations at recharge $C_i$. The potential $^{36}Cl$ evolutionary pathways are depicted in Figure 10 where the $^{36}Cl/Cl$ ratios are plotted as function of the $^{36}Cl$ concentration. Also shown are the $^{36}Cl/Cl$ signatures of ERR, precipitation and data from other studies in the area (Love et al., 2000). Those data indicate diffuse recharge with a high initial ratio $R_i$ first followed by evaporative enrichment and then followed by a combination of Cl accumulation in the subsurface and radioactive decay (indicated by arrows in Figure 10). The exact pathways to the data points are ambiguous without additional data (i.e., the solid and dashed paths in Figure 10 are both possible). However, since evaporative enrichment for ERR is limited (crossed out arrow in the figure), it is clear, that data of group 2-3 must partly originate from diffuse recharge which is characterised be high a $^{36}Cl/Cl$ ratio of $120\times10^{-15}$ and elevated Cl concentration (and thus high $N_{36Cl}$). With that, a new $^{36}Cl$ budget can be formulated in which the $^{36}Cl$ contributions from ERR and diffuse recharge are separated:

$$R \cdot C = (R_{ERR} \cdot C_{ERR} + R_D \cdot C_D) \cdot \exp(-\lambda_{36} \cdot t) + R_{Se} \cdot C / 2 \cdot \left(1 - \exp(-\lambda_{36} \cdot t)\right) + (C - C_D - C_{ERR}) \cdot R_{ex}$$

Eq 7

The second term describes the ingrowth to secular production-decay equilibrium $R_{se}$ in the aquifer which also depends on the timing of the increase of Cl along the flow path which is *a priori* unknown. The factor of two assumes an $^{36}$Cl in-situ production rate corresponding to a time averaged Cl concentration of C/2. Equation 7 can be solved for the concentration $C_D$ contributed from diffusive recharge:

$$C_D(t) = \frac{C\left(R - R_{SE} / 2\right) \cdot \left(1 - \exp(-\lambda_{36} \cdot t)\right) - R_{ERR} \cdot C_{ERR} \cdot \exp(-\lambda_{36} \cdot t) - (C - C_{ERR}) \cdot R_{Ex}}{(R_D \cdot \exp(-\lambda_{36} \cdot t) - R_{EX})} \qquad \text{Eq 8}$$

Figure 9 shows the resulting $C_D(t)$ and $C_a(t)=C-C_{ERR}-C_D(t)$ as function of the $^{81}$Kr ages. Cl accumulation in the subsurface contributes about 1/3 to the observed Cl increase along the flow path. The chloride accumulation rate of ~1.8 ± 1 mg/L kyr is consistent with values found in other studies in the western GAB (Lehmann et al., 2003; Love et al., 2000). Up to 400 mg/L Cl are attributed to changes on the initial Cl concentration at recharge $C_D$, which first increases with groundwater age but levels off for the oldest waters as indicated in the figure. The groundwaters sampled towards the centre of the basin (group 2-3) are partly originating from areas with diffuse recharge under varying climatic conditions. This is strongly supported by the stable isotope data shown in Figure 4a where a strong correlation between $\delta^{18}$O values and $C_D$ can be observed. Group 1 samples fall along the LMWL and are isotopically depleted. Moving away from the Finke River recharge plume, the isotope signature becomes more enriched along a line with slope 6.4. This correlation might be partly caused by evaporation but is rather a mixing line than a evaporation line as demonstrated in Figure 4b. The shift in the stable isotope signature parallels an increase of the initial Cl concentration $C_D$. Also shown are calculated evaporation and transpiration trends. Transpiration will increase the chloride concentration without affecting the $\delta^{18}$O but unrealistic large fractions of water need to be transpired to explain the observed scatter

(Sultan et al., 2000). The slope of the evaporation line is too small to explain the observed variation in Cl concentration. This suggests that mixing of water that recharged at different conditions is going on and/or the additions of salt come from dust solutes dissolved during the recharge process (Sultan et al., 2000).

Sample 19, for example, which has one of the highest Cl concentrations and a higher Cl accumulation rate is geographically separated from the main transect towards the south. According to the recent piezometric head distribution (Figure 1) the water originates from a recharge area further south where there is no evidence for any ERR source water (Love et al., 2000) and Figure 10.

## *5.5 Origin and rate of accumulated Helium*

The isotope signature of accumulated helium indicates two 2 distinct endmembers: atmospheric helium with a $^3He/^4He$ ratio of air saturated water (ASW) ($1.36 \times 10^{-6}$) plus a radiogenic component (Figure 11a). A linear fit in the $^3He/^4He$ vs. $Ne/^4He$ plot reveals a ratio of $1.5 \times 10^{-8}$ for the radiogenic components which is typical for crustal production (Stute et al., 1992). No mantle helium contribution is indicated by the data.

Using the Ne excess ($\Delta Ne$) from excess air (Table 2) and assuming a recharge temperature and elevation of 20°C and 400 meters respectively, the fraction of radiogenic $^4He_{rad}$ can be calculated (Kipfer et al., 2002) which is plotted in Figure 11b as a function of $^{81}Kr$ derived tracer ages. There is a systematic increase of $^4He_{rad}$ with increasing $^{81}Kr$ age which highly supports the chronology of $^{81}Kr$ ages and is indicative for a relatively homogeneous groundwater flow path. The $^4He$ in-situ accumulation rate ($A_{He}$) can be calculated based on the [U] and [Th] concentrations of the aquifer rocks of 0.8 ppm and 6 ppm respectively (Andrews and Lee, 1979; Lehmann et al., 2003), an aquifer density of $\rho$=2.6 g/cm$^3$, a porosity of $\phi$=0.2, and a helium release factor of 1 into the water filled pore space (Mazor and Bosch, 1992).

$$A_{He}=\rho/\phi\ (1.19\ 10^{-13}\ [U] +2.88\ 10^{-14}\ [Th]) \qquad \text{Eq. 9}$$

The resulting helium in situ accumulation rate $A_{He}$ of 4 x $10^{-12}$ $cm^3_{STP}/g_w/yr$, is depicted in Figure 11b.

It is obvious that in-situ production is not sufficient to explain the observed $^4He$ increase rate, a situation found in other aquifers (Aggarwal et al., 2015; Torgersen, 2010; Torgersen and Clarke, 1985). In particular for the samples further away from the recharge area (group 2-3 waters), the helium accumulation rate exceeds the expected value from in-situ production by almost two orders of magnitude, which is in line with observations made in other parts of the GAB. Torgersen and Ivey, (1985) proposed a model in which an external $^4He$ flux of 3 x $10^{-6}$ $cm^3_{STP}/cm^2/yr$ originating from the underlying strata enters the aquifer from below. Their model assumes a transversal dispersion coefficient of 0.1 $m^2/yr$ and $^4He$ no-flow upper boundary (Torgersen and Ivey, 1985). This leads to a nonlinear $^4He$ accumulation rate with age and flow distance with a transition from an in-situ accumulation rate to an accumulation rate determined by the basal $^4He$ flux strength. The point in time (and flow distance) where the transition occurs is determined by the depth of the screened borehole interval in relation to the total depth of the aquifer. A borehole that intersects only the upper part of the aquifer "sees" the basal $^4He$ flux later than a well completed deeper in the formation. The corresponding model line for an aquifer thickness H = 400 m and a well tapping to the top layer of the aquifer is shown in Figure 11b. There is a reasonable agreement between the Torgersen and Ivy model and the data, also the transition point to the higher accumulation rate between groups 1 and 2 waters is well represented. Thus, our $^{81}Kr$ data support the general concept of a (crustal) He influx as developed in the past at other parts of the GAB(Torgersen and Clarke, 1985; Torgersen and Ivey, 1985). Other scenarios where e.g. the source of $^4He$ (and chloride) occurs in the overlying Bulldog Shale (Lehmann et al., 2003; Love et al., 2000) or in impermeable layers within the aquifer which pre-accumulated $^4He$ in the past cannot be completely excluded but are less supported by the data. The good correlation between the concentration of radiogenic helium $^4He_{rad}$ and the reconstructed chloride accumulation ($C_a$) points to a common source and transport process of helium and chloride (Figure 11c) (Lehmann et al., 2003; Zhang et al., 2007)

# 6 Conclusions

The quantification and reconstruction of amount and mechanism of groundwater recharge in arid areas is fundamental for the life and economies in those areas. Such aquifers typically include a very large range of groundwater residence times and different climatic zones in the recharge regimes over time. However, the characterisation of the age structure of groundwater over extended spatial and temporal scales is a very difficult task. Various tracers need to be combined which cover different dating ranges, but which are also affected by different process that may affect the interpretation in terms of groundwater residence times. One of these is changing recharge conditions which can only be deconvoluted if multiple tracers covering the same time scales are applied. In this study a complete tracer set in incrementally increasing half-lives and dating ranges from decades to millions of years was applied to a large aquifer along a presumed groundwater flow path. In order of increasing dating range this includes the measurements of $^{85}Kr$, $^{39}Ar$, $^{14}C$, $^{81}Kr$, $^{36}Cl$ and $^{4}He_{rad}$. This unique combination with partly overlapping and complementing dating ranges allows for a deeper understanding of the hydrogeology of the studied area, and also for the first time, for a comprehensive comparison and assessment of the age information obtained by different applied dating methods.

Generally, the data indicate a consistent age chronology with distance from the Finke River recharge area. The continued increase of groundwater residence times with distance from the Finke River implies the existence of a connected flow system in contrast to the possibility of having partly isolated subsystems. Flow velocities determined by the spatial gradients of the concentrations of $^{39}Ar$, $^{14}C$ and $^{81}Kr$ decrease with increasing half-life of the used tracer and thus with increasing distance from recharge area. Despite the inherent uncertainties of the individual dating methods this is attributed to a diverging mass flow from a localized recharge point. In the investigated western part of the GAB ERR was the dominant recharge mechanism over long timescales. In the down gradient part of the system where groundwater residence times exceed 100,000 years as indicated by the $^{81}Kr$ data the influence and contribution of ERR becomes less important due to the admixture of water originating from other recharge areas. At such timescales transient recharge conditions,

water rock interaction, hydrodynamic dispersion and diffusive exchange with the aquitards become increasingly important. As already pointed out in other studies (Phillips, 2000; Phillips et al., 1986) the application of $^{36}Cl$ for old groundwater dating is highly complicated in this part of the GAB because the initial parameters $R_i$ and $C_i$ are not well defined and variable due the multitude of processes and recharge mechanisms which may affect those parameters.

The $^{81}Kr$ dating methods allowed deconvoluting the complicated $^{36}Cl/Cl$ systematics in this part of the GAB. The $^{36}Cl$ data underpin the decreasing influence of ERR towards the centre of the basin, where groundwater originating from diffuse recharge becomes more important. Varying recharge conditions and related recharge mechanisms are also reflected in variations of the stable isotope signature of the water molecule and the chloride concentration at recharge. However, more than 50% of the observed chloride increase along the flow line is caused by subsurface processes. This Cl accumulation rate is accompanied by increasing $^{4}He_{rad}$ concentrations. The rate as well as the temporal and spatial pattern of the $^{4}He$ concentrations is in good agreement with the assumption of a previously postulated crustal helium flux entering the system from underlying strata. Diffusive exchange with those layers may also affect the $^{81}Kr$ ages but was neglected in this study (Purtschert et al., 2013). This work also demonstrates the potential of very old groundwater as an archive of paleoclimate conditions over long timescales. The $^{81}Kr$ dating method not only provides a reliable age chronology but also increases the potential for meaningful climate proxies such as the Cl and stable isotope concentration at time of recharge.

# 7 Acknowledgements

This study was partly funded by the National Water Commission of Australia under the project Allocating Water and Maintaining Springs in the Great Artesian Basin and by the U.S. DOE, Office of Science, Office of Nuclear Physics, under contract DE-AC02-06CH11357. We also thank the Swiss Science Foundation for financial support (Grant number 200020_172550). Thanks to Philip Paterson, for his invaluable help in the field. We thank K. Sasa and T Takahashi for measuring $^{36}Cl/Cl$. We acknowledge the valuable commends and careful reviews of two anonymous reviewers which helped to improve this manuscript.

# 8 References


Aeschbach-Hertig, W. and Solomon, D.K. (2013) Noble Gas Thermometry in Groundwater Hydrology, in: Burnard, P. (Ed.), The Noble Gases as Geochemical Tracers. Springer Berlin Heidelberg, Berlin, Heidelberg, pp. 81-122.

Aggarwal, P.K., Araguas-Araguas, L., Choudhry, M., van Duren, M. and Froehlich, K. (2014) Lower Groundwater 14C Age by Atmospheric CO2 Uptake During Sampling and Analysis. Groundwater 52, 20-24.

Aggarwal, P.K., Fröhlich, K., Glynn, P.D., Phillips, F.M., Plummer, L.N., Purtschert, R., Reilly, T.E., Sanford, W., Sturchio, N.C., Stute, M., Suckow, A., Torgersen, T. and Yokochi, R. (2013) Isotope methods for dating old groundwater. International Atomic Energy Agency, Vienna.

Aggarwal, P.K., Matsumoto, T., Sturchio, N.C., Chang, H.K., Gastmans, D., Araguas-Araguas, L.J., Jiang, W., Lu, Z.-T., Mueller, P., Yokochi, R., Purtschert, R. and Torgersen, T. (2015) Continental degassing of 4He by surficial discharge of deep groundwater. Nature Geosci 8, 35-39.

Andrews, J.N. and Lee, D.J. (1979) Inert gases in groundwater from the Bunter Sandstone of England as indicators of age and palaeoclimatic trends. J Hydrol 41, 233-252.

Aoki, N. and Makide, Y. (2005) The Concentration of Krypton in the Atmosphere—Its Revision after Half a Century. Chemistry Letters 34, 1396.

Bentley, H.W., Phillips, F., Davis, S.N., Habermehl, M.A., Airey, P.L., Calf, G.E., Elmore, D., Gove, H. and Torgersen, T. (1986a) Chlorine 36 dating of very old groundwater: The Great Arthesian Basin, Australia. Water Resources Reseach 22, 1991-2001.

Bentley, H.W., Phillips, F.M., Davis, S.N., Habermehl, M.A., Airey, P.L., Calf, G.E., Elmore, D., Gove, H.E. and Torgersen, T. (1986b) Chlorine 36 Dating of Very Old Groundwater 1. The Great Artesian Basin, Australia. Water Resources Research 22, 1991-2001.

Beyerle, U., Aeschbach-Hertig, W., Imboden, D.M., Baur, H., Graf, T. and Kipfer, R. (2000) A mass spectrometric system for the analysis of noble gases and tritium from water samples. Environ. Sci. Technol. 34, 2042-2050.

Buizert, C., Bagenstoss, D., Jiang, W., Purtschert, R., Petrenko, V., Brook, E., Lu, Z.T., Müller, P. and Severinghaus, J.P. (2013) Radiometric 81Kr dating reveals 120,000 year old ice at Taylor Glacier, Antarctica, Goldschmidt, Florence.

Collon, P., Kutschera, W., Loosli, H.H., Lehmann, B.E., Purtschert, R., Love, A., Sampson, L., Anthony, D., Cole, D. and Davids, B. (2000) 81Kr in the Great Artesian Basin, Australia: a new method for dating very old groundwater. Earth and Planetary Science Letters 182, 103-113.

Du, X., Purtschert, R., Bailey, K., Lehmann, B.E., Lorenzo, R., Lu, Z.T., Mueller, P., O'Connor, T.P. and Sturchio, N.C. (2003) A new method of measuring 81Kr and 85Kr abundances in environmental samples. Geophysical Research Letters 30, 2068.

Fulton, S., Wohling, D., Love, A.J. and Berens, V. (2013) Diffuse Recharge - Allocating Water and Maintaining Springs in the Great Artesian Basin: chapter 3

Ephemeral river recharge, in: Commission, N.W. (Ed.), Groundwater Recharge, Hydrodynamics and Hydrochemistry of the Western Great Artesian Basin.

Gerber, C., Vaikmäe, R., Aeschbach, W., Babre, A., Jiang, W., Leuenberger, M., Lu, Z.-T., Mokrik, R., Müller, P., Raidla, V., Saks, T., Waber, H.N., Weissbach, T., Zappala, J.C. and Purtschert, R. (2017) Using 81Kr and noble gases to characterize and date groundwater and brines in the Baltic Artesian Basin on the one-million-year timescale. Geochimica et Cosmochimica Acta 205, 187-210.

Habermehl, M.A. (1980) The Great Artesian Basin, Australia. Journal of Australian Geology & Geophysics 5, 9-38.

Jiang, W., Bailey, K., Lu, Z.T., Mueller, P., O'Connor, T.M., Chen, C.F., Hu, S.-M., Purtschert, R., Sturchio, N.C., Sun, Y.R., Williams, W.D. and Yang, G.-M. (2012) An Atom Counter for Measuring 81Kr and 85Kr in Environmental Samples. Geochem. Cosmochim. Acta 91, 1-6.

Jiang, W., Hu, S.-M., Lu, Z.-T., Ritterbusch, F. and Yang, G.-m. (2020) Latest development of radiokrypton dating – A tool to find and study paleogroundwater. Quaternary International 547, 166-171.

Kipfer, R., Aeschbach Hertig, W., Peeters, F. and Stute, M. (2002) Noble Gases in Lakes and Ground Waters, in: Porcelli, D., Ballentine, C.J., Wieler, R. (Eds.), Noble Gases in Geochemistry and Cosmochemistry. Geochemical Society

Mineralogical Society of America, pp. 615-690.

Lehmann, B.E., Davis, S.N. and Fabryka Martin, J.T. (1993) Atmospheric and subsurface sources of stable and radioactive nuclides used for groundwater dating. Water Resources Research 29, 2027-2040.

Lehmann, B.E., Love, A., Purtschert, R., Collon, P., Loosli, H., Kutschera, W., Beyerle, U., Aeschbach Hertig, W., Kipfer, R., Frape, S.K., Herczeg, A.L., Moran, J., Tolstikhin, I. and Groening, M. (2003) A comparison of groundwater dating with $^{81}Kr$, $^{36}Cl$ and $^{4}He$ in four wells of the Great Artesian Basin, Australia. Earth and Planetary Science Letters 211, 237-250.

Loosli, H.H. (1983) A dating method with 39Ar. Earth and Planetary Science Letters 63, 51-62.

Loosli, H.H. and Purtschert, R. (2005) Rare Gases, in: Aggarwal, P., Gat, J.R., Froehlich, K. (Eds.), Isotopes in the Water Cycle: Past, Present and Future of a Developing Science. IAEA, Vienna, pp. 91-95.

Love, A.J., Herczeg, A.L., Samson, L., Cresswell, R.G. and Fifield, L.K. (2000) Sources of chloride and implications for 36Cl dating of old groundwater, South Western Great Artesian basin, Australia. Water Res. Res. 36, 1561-1574.

Love, A.J., Wohling, D., Fulton, S., Love, A.J., Scanlon, B., Rousseau-Gueutin, P. and DeRitter, S. (2013) Diffuse Recharge - Allocating Water and Maintaining Springs in the Great Artesian Basin: , in: Commission, N.W. (Ed.), Groundwater Recharge, Hydrodynamics and Hydrochemistry of the Western Great Artesian Basin.

Lu, Z.T., Schlosser, P., Smethie Jr, W.M., Sturchio, N.C., Fischer, T.P., Kennedy, B.M., Purtschert, R., Severinghaus, J.P., Solomon, D.K., Tanhua, T. and Yokochi, R. (2014) Tracer applications of noble gas radionuclides in the geosciences. Earth-Science Reviews.

Matsumoto, T., Chen, Z., Wei, W., Yang, G.-M., Hu, S.-M. and Zhang, X. (2018) Application of combined 81Kr and 4He chronometers to the dating of old groundwater in a tectonically active region of the North China Plain. Earth and Planetary Science Letters 493, 208-217.

Mazor, E. and Bosch, A. (1992) Helium as a semi-quantitative tool for groundwater dating in the range of 104-108 years. IAEA, International Atomic Energy Agency (IAEA).

Phillips, F. (2000) Chlorine-36, in: Cook, P.G., Herczeg, A.L. (Eds.), Environmental Tracers in Subsurface Hydrology. Kluwer, Boston, pp. 379-396.

Phillips, F.M., Bentley, H.W., Davis, S.N., Elmore, D. and Swanick, G.B. (1986) Chlorine 36 dating of very old groundwater 2. Milk River Aquifer, Alberta, Canada. Wat. Resour. Res. 22, 2003-2016.

Priestley, S.C., Love, A.J., Post, V., Shand, P., Wohling, D., Kipfer, R., Payne, T.E., Stute, M. and Tyroller, L. (2017) Environmental Tracers in Groundwaters and Porewaters to Understand Groundwater Movement Through an Argillaceous Aquitard. Procedia Earth and Planetary Science 17, 420-423.

Purtschert, R., Sturchio, N.C. and Yokochi, R. (2013) Krypton-81 dating of old groundwater in: Suckow, A., Aggarwal, P., Araguas-Araguas, L. (Eds.), Isotope methods for dating old groundwater. IAEA, Vienna, pp. 91-124.

Purtschert, R., Yokochi, R., Jiang, W., Lu, Z.T., Mueller, P., Zappala, J., Van Heerden, E., Cason, E., Lau, M., Kieft, T.L., Gerber, C., Brennwald, M.S. and Onstott, T.C. (2021) Underground production of 81Kr detected in subsurface fluids. Geochimica et Cosmochimica Acta 295, 65-79.

Radke, B.M. and Sciences, A.B.o.R. (2000) Hydrochemistry and Implied Hydrodynamics of the Cadna-owie - Hooray Aquifer, Great Artesian Basin, Australia. Bureau of Rural Sciences.

Ram, R., Purtschert, R., Adar, E.M., Bishof, M., Jiang, W., Lu, Z.-T., Mueller, P., Sy, A., Vockenhuber, C., Yechieli, Y., Yokochi, R., Zappala, J.C. and Burg, A. (2021) Controls on the 36Cl/Cl input ratio of paleo-groundwater in arid environments: New evidence from 81Kr/Kr data. Science of The Total Environment 762, 144106.

Rousseau-Gueutin, P., Love, A.J., Vasseur, G., Robinson, N.I., Simmons, C.T. and de Marsily, G. (2013) Time to reach near-steady state in large aquifers. Water Resources Research 49, 6893-6908.

Sasa, K., Takahashi, T., Tosaki, Y., Matsushi, Y., Sueki, K., Tamari, M., Amano, T., Oki, T., Mihara, S., Yamato, Y., Nagashima, Y., Bessho, K., Kinoshita, N. and Matsumura, H. (2010) Status and research programs of the multinuclide accelerator mass spectrometry system at the University of Tsukuba. Nuclear Instruments and Methods in Physics Research Section B: Beam Interactions with Materials and Atoms 268, 871-875.

Sturchio, N.C., Du, X., Purtschert, R., Lehmann, B., Sultan, M., Patterson, L.J., Lu, Z.-T., Müller, P., Bigler, T., Bailey, K., O'Connor, T.P., Young, L., Lorenzo, R., Becker, R., El Alfy, Z., El Kaliouby, B., Dawood, Y. and Abdallah, A.M.A. (2004) One million year old groundwater in the Sahara revealed by krypton-81 and chlorine-36. Geophys. Res. Lett. 31, L05503.

Sturchio, N.C., Kuhlman, K.L., Yokochi, R., Probst, P.C., Jiang, W., Lu, Z.-T., Mueller, P. and Yang, G.-M. (2014) Krypton-81 in groundwater of the Culebra Dolomite near the Waste Isolation Pilot Plant, New Mexico. Journal of Contaminant Hydrology 160, 12-20.

Stute, M., Sonntag, C., Déak, J. and Schlosser, P. (1992) Helium in deep circulating groundwater in the Great Hungarian Plain: Flow dynamics and crustal and mantle helium fluxes. Geochimica et Cosmochimica Acta 56, 2051-2067.

Sultan, M., Sturchio, N.C., Gheith, H., Hady, Y.A. and El Arkeawy, M. (2000) Chemical and Isotopic Constraints on the Origin of Wadi El-Tarfa Ground Water, Eastern Desert, Egypt. Groundwater 38, 743-751.

Torgersen, T. (2010) Continental degassing flux of 4He and its variability. Geochemistry, Geophysics, Geosystems 11, n/a-n/a.

Torgersen, T. and Clarke, W.B. (1985) Helium accumulation in groundwater, I: An evaluation of sources and the continental flux of crustal $^4$He in the Great Artesian Basin, Australia. Geochimica et Cosmochimica Acta 49, 1211-1218.

Torgersen, T. and Clarke, W.B. (1987) Helium accumulation in groundwater, III. Limits on helium transfer across the mantle-crust boundary beneath Australia and the magnitude of mantle degassing. Earth Planet. Sci. Lett. 84, 345-355.

Torgersen, T., Habermehl, M.A., Phillips, F.M., Elmore, D., Kubik, P., Jones, B.G. and Hemmick, T. (1991) Chlorine 36 dating of very old groundwater 3. Further studies in the Great Artesian Basin. Wat. Res. Res. 27, 3201-3213.

Torgersen, T. and Ivey, G.N. (1985) Helium accumulation in groundwater, II: A model for the accumulation of the crustal $^4$He degassing flux. Geochimica et Cosmochimica Acta 49, 2445-2452.

Tosaki, Y., Tase, N., Kondoh, A., Sasa, K., Takahashi, T. and Nagashima, Y. (2011) Distribution of 36Cl in the Yoro River Basin, Central Japan, and Its Relation to the Residence Time of the Regional Groundwater Flow System. Water 3, 64.

Winger, K., Feichter, J., Kalinowski, M.B., Sartorius, H. and Schlosser, C. (2005) A new compilation of the atmospheric 85krypton inventories from 1945 to 2000 and its evaluation in a global transport model. Journal of Environmental Radioactivity 80, 183-215.

Wohling, D., Fulton, S., Love, A.J. and Scanlon, B. (2013) Diffuse Recharge - Allocating Water and Maintaining Springs in the Great Artesian Basin: Chapter 2: Diffusive recharge, in: Commission, N.W. (Ed.), Groundwater Recharge, Hydrodynamics and Hydrochemistry of the Western Great Artesian Basin.

Yechieli, Y., Yokochi, R., Zilberbrand, M., Lu, Z.-T., Purtschert, R., Sueltenfuss, J., Jiang, W., Zappala, J., Mueller, P., Bernier, R., Avrahamov, N., Adar, E., Talhami, F., Livshitz, Y. and Burg, A. (2019)

Recent seawater intrusion into deep aquifer determined by the radioactive noble-gas isotopes 81Kr and 39Ar. Earth and Planetary Science Letters 507, 21-29.

Yokochi, R., Bernier, R., Purtschert, R., Zappala, J.C., Yechieli, Y., Adar, E., Jiang, W., Lu, Z.-T., Mueller, P., Olack, G. and Ram, R. (2017) Field Degassing as a New Sampling Method for 14C Analyses in Old Groundwater. Radiocarbon 60, 349-366.

Yokochi, R., Ram, R., Zappala, J.C., Jiang, W., Adar, E., Bernier, R., Burg, A., Dayan, U., Lu, Z.-T., Mueller, P., Purtschert, R. and Yechieli, Y. (2019) Radiokrypton unveils dual moisture sources of a deep desert aquifer. Proceedings of the National Academy of Sciences 116, 16222.

Yokochi, R., Zappala, J.C., Purtschert, R. and Mueller, P. (2021) Origin of water masses in Floridan Aquifer System revealed by 81Kr. Earth and Planetary Science Letters 569, 117060.

Zappala, J.C., Baggenstos, D., Gerber, C., Jiang, W., Kennedy, B.M., Lu, Z.T., Masarik, J., Mueller, P., Purtschert, R. and Visser, A. (2020) Atmospheric 81Kr as an integrator of cosmic-ray flux on the hundred-thousand-year timescale. Geophysical Research Letters n/a, e2019GL086381.

Zhang, M., Frape, S., Love, A., Herczeg, A.L., Lehmann, B.E., Beyerle, U. and Purtschert, R. (2007) Chlorine stable isotope studies of old groundwater, southwestern Great Artesian Basin, Australia. Appl. Geochemistry 22, 557-574.

Zhang, Z.Y., Ritterbusch, F., Hu, W.K., Dong, X.Z., Gao, C.Y., Jiang, W., Liu, S.Y., Lu, Z.T., Wang, J.S. and Yang, G.M. (2020) Enhancement of the 81Kr and 85Kr count rates by optical pumping. Physical Review A 101, 053429.

Zuber, A., Rozanski, K., Kaniac, J. and Purtschert, R. (2010) On some methodological problems in the use of environmental tracers to estimate hydrogeologic parameters and to calibrate flow and transport models. Hydrogeology Journal 19, 53-69.

# 9 Tables

| Sample No. | Local Name | Temperature °C | Specific EC (µS/cm) | Cl mg/L | $\delta^{18}O$ ‰ | $\delta^{2}H$ ‰ | $\delta^{13}C$ ‰ |
|---|---|---|---|---|---|---|---|
| 1 | | 29.08 | 666 | 84 | -10.3 | -71.8 | -11.4 |
| 2 | New Townsend | 29.06 | 595 | 86 | -9.8 | -67.8 | -10.8 |
| 3 | Sandy Bore | 28.83 | 755 | 130 | -8.9 | -63.1 | -10.3 |
| 4 | Roads Bore | 33.14 | 3017 | 760 | 8.3 | -58.8 | -9.7 |
| 5 | Maryanne Stock Bore | 30.25 | 1303 | 250 | -9.6 | -66.9 | -10.5 |
| 6 | Willoughby Bore | 29.35 | 582 | 8[illegible] | -9.4 | -66.8 | -10.6 |
| 7 | | 28.72 | 781 | 1[illegible]0 | -10.6 | -73.6 | -11.6 |
| 8 | Bore 8 (Finke) | 28.04 | 801 | [illegible]50 | -9.4 | -65.1 | -13.3 |
| 9 | Mt Dare HS | 41.86 | 1489 | 280 | -8.4 | -57.6 | -10.7 |
| 10 | 3 O'Clock Creek Bore | 40.57 | 163[illegible] | 330 | -7.5 | -53.3 | -11.0 |
| 11 | Junction Bore | 46.04 | 2136 | 440 | -6.8 | -50.7 | -11.7 |
| 12 | Stevensons Bore | 46.27 | [illegible]246 | 670 | -6.6 | -49.3 | -11.7 |
| 13 | Oodnadatta #3 | 41.81 | 29[illegible]8 | 630 | -6.85 | -48.8 | -11.7 |
| 14 | Snake Creek No.2 | 60.4 | 4335 | 950 | -6.4 | -44.9 | -11.0 |
| 15 | Horseshoe Bore 2 | 38.08 | 4090 | 950 | -5.9 | -43.5 | |
| 16 | Apperinna Bore 2 | 49.8[illegible] | 3609 | 810 | -6.6 | -49.2 | -10.3 |
| 17 | Duckhole No. 2 | 38.8[illegible] | 3704 | 830 | -6.8 | -47.8 | -9.9 |
| 18 | Watson Creek 2 | 39.94 | 4417 | 1100 | -6.5 | -44.4 | -9.3 |
| 19 | Raspberry Creek 2 | 29.36 | 5032 | 1200 | -6.11 | -45.7 | -8.2 |

**Table 1**: For well locations we refer to Figure 1. Bore type S (stock), M (monitoring) and T (small town supply). Bores 1-8 are unconfined, while bores 9-19 are confined. Field parameters, Chloride, and stable isotopes of the water molecule and stable Carbon 13.

| Sample. No. | $^{39}$Ar pmAr | $^{85}$Kr dpm/cc$_{Kr}$ | $^{81}$Kr pmKr | $^{14}$C pmC | $^{36}$Cl/Cl ×10$^{-15}$ | $^{3}$He/$^{4}$He ×10$^{-8}$ | $^{4}$He cm$^{3}_{STP}$/g×10$^{-8}$ | ΔNe % | $^{39}$Ar$_{age}$ yrs | $^{14}$C$_{age}$ kyr | $^{81}$Kr$_{age}$ kyr |
|---|---|---|---|---|---|---|---|---|---|---|---|
| 1 | <10 | 1.6 ± 0.6 | 98 ± 7 | 74.5 | 55 ± 4 | 147.3 | < 0.2 | 58.2 | >894 | 1.2 | 6.7 |
| 2 | 24 ± 6 | <0.9 | 100 ± 7 | 84.64 | 61 ±4 | 158.6 | < 0.2 | 37.[illegible] | 550 ± 100 | 0.1 | 0.5 |
| 3 | 55 ±6 | <1.5 | 85 ± 7 | 82.08 | 91 ± 5 | 149.2 | < 0.2 | 20.5 | 230 ± 40 | 0.4 | 51.8 |
| 4 | <4 | 0.8 ± 0.5 | 99 ± 8 | 17.65 | 38 ± 3 | 85 | 6.1 ± 0.2 | 65.[illegible] | > 1249 | 14.8 | 3.3 |
| 5 | 26±7 | < 0.9 | 107 ± 8 | 42.09 | 61 ± 4 | 116 | 0.8 ± 0.1 | 54.7 | 520 ± 100 | 6.3 | 0.5 |
| 6 | <6 | 1.2 ± 0.5 | 91 ± 8 | 67.43 | 52 ± 4 | 148.1 | < 0.2 | 7.6 | >1092 | 2.1 | 31.2 |
| 7 | 19 ±8 | 34.0 ± 2.6 | 72 ± 9 | 63.07 | 57 ± 4 | 136.7 | < 0.[illegible] | 155.3 | 645 ± 160 | 2.7 | |
| 8 | 65 ±7 | 1.8 ± 0.6 | 105 ± 7 | 89.94 | | 160 | < 0.2 | 60.7 | > 167 | -0.4 | 0.5 |
| 9 | <8 | 10.3 ± 0.9* | 87±7 | 9.94 | 73 ± 4 | 32.4 | 32 ± 0.5 | 77.6 | > 980 | 21.7 | 112.9 |
| 10 | <14 | < 0.8 | 82 ± 7 | 4.74 | 49 ± 5 | 9.3 | 176.8 ± 2.3 | 83.1 | > 763 | 38.8 | 65.6 |
| 11 | <5 | 1.2 ± 0.6 | 69 ± 6 | 7.74 | 49 ± 5 | 4.7 | 377.2 ± 5.4 | 52.4 | > 1163 | 25.5 | 122.6 |
| 12 | 87 ±7 | <1.1 | 56 ± 5 | 2.59 | 62 ± 4 | 1.8 | 1650 ± 20.4 | 61.1 | 50 ± 20 | >40 | 191.6 |
| 13 | <10 | 1.2 ± 0.5 | 81 ± 8 | 4.73 | 55 ± 3 | 2.6 | 1287 ± 16.3 | 75.9 | >894 | 39.0 | 69.6 |
| 14 | <4 | 12.3 ± 1.2* | 47±6/37±7 | 5.37 | 34 ± 2 | 0.9 | 5341 ± 0.7 | 38.1 | > 1249 | 33.8 | 427.9 |
| 15 | <10 | 40 ± 3 | 92 ± 10 | [illegible] | 37 ± 3 | 1.4 | 4759. ± 52 | 40.8 | >894 | - | |
| 16 | <3 | 0.8 ± 0.5 | 36 ± 5 | 2.57 | 27 ± 2 | 2.2 | 2831 ± 35 | 50.8 | >1361 | >40 | 337.5 |
| 17 | <10 | <1.5 | 47 ± 5 | 6.84 | 32 ± 2 | 1.4 | 3981 ± 43 | 49.3 | >894 | 27.7 | 249.4 |
| 18 | <8 | <1.1 | 34 ± 4 | 4.95 | 17 ± 2 | 1.4 | 6509 ± 73 | 36.6 | >980 | 36.8 | 356.4 |
| 19 | <10 | 1.3 ± 0.6 | 87 ± 8 | 4.34 | 53 ± 4 | | | | >894 | 45.3 | 46 |

**Table 2**: Dating tracers, Helium data and decay tracer residence times. *$^{85}$Kr activities interpreted as contamination and used for $^{81}$Kr correction

| Parameter | Value |
|---|---|
| $R_{SE}$ | $6.5 \times 10^{-15}$ |
| $R_{EX}$ | $10 \times 10^{-15}$ |
| $R_{ERR}$ | $60 \times 10^{-15}$ |
| $R_D$ | $120 \times 10^{-15}$ |
| $C_{ERR}$ | 100 mg/L |

**Table 3**: $^{36}Cl$ and Cl parameters used in Eq. 8, where $R_{SE}$ = is the $^{36}Cl/Cl$ in secular equilibrium with the J sandstone aquifer $R_{EX}$ is the $^{36}Cl/Cl$ of the secular equilibrium of the external source $R_{ERR}$ is the $^{36}Cl/Cl$ input ratio of the ephemeral river recharge, $R_D$ is the $^{36}Cl/Cl$ input ratio of diffuse recharge component, and $C_{ERR}$ is the initial Cl concentration of the ephemeral river recharge.

# 10 Figures

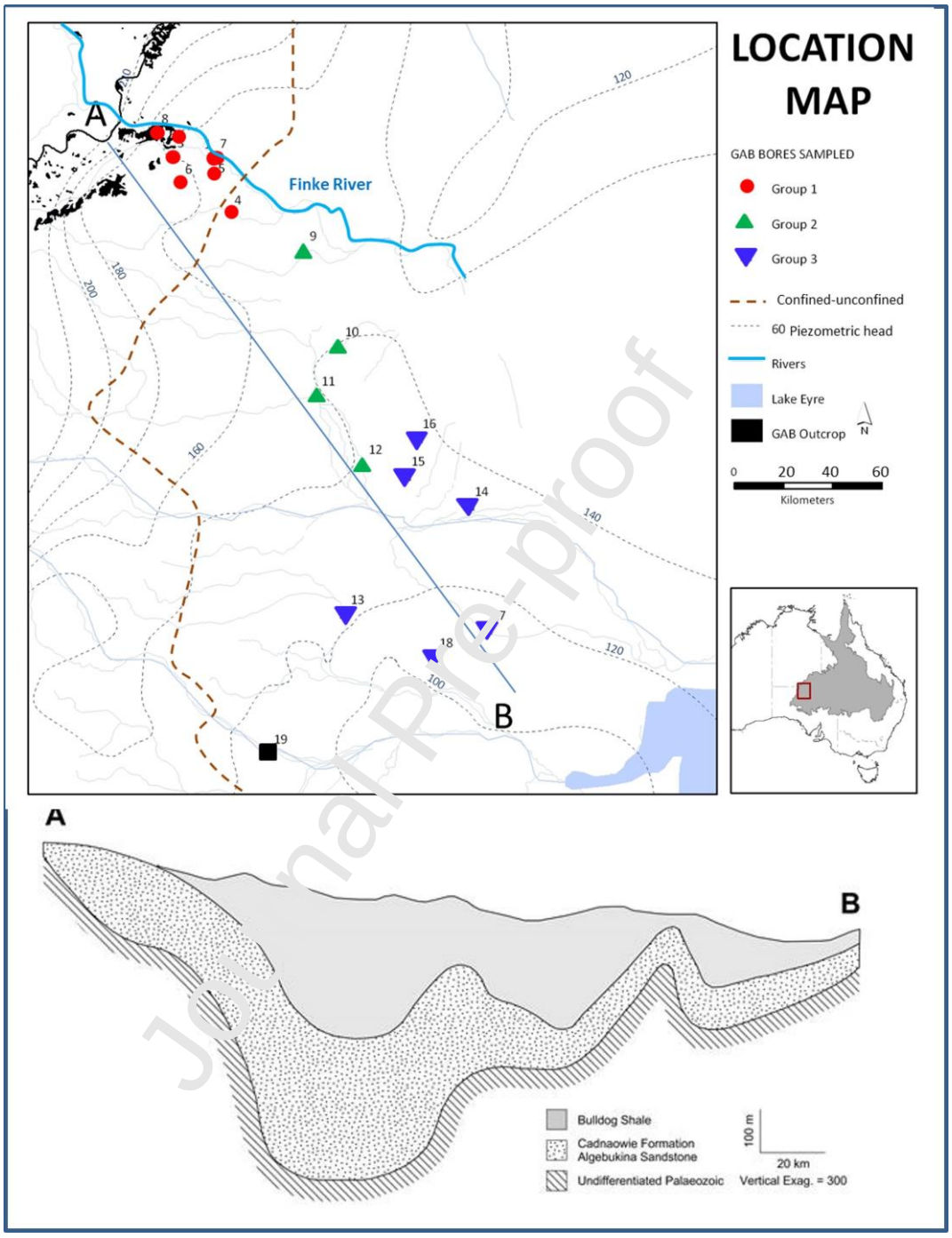


Figure 1. Map of the study area showing the different groundwater groups. The dashed line represents the potentiometric contours (Rousseau-Gueutin et al 2013) where the generalised direction of groundwater flow is at right angles to these contour lines. A-B represents the hydrogeological cross section

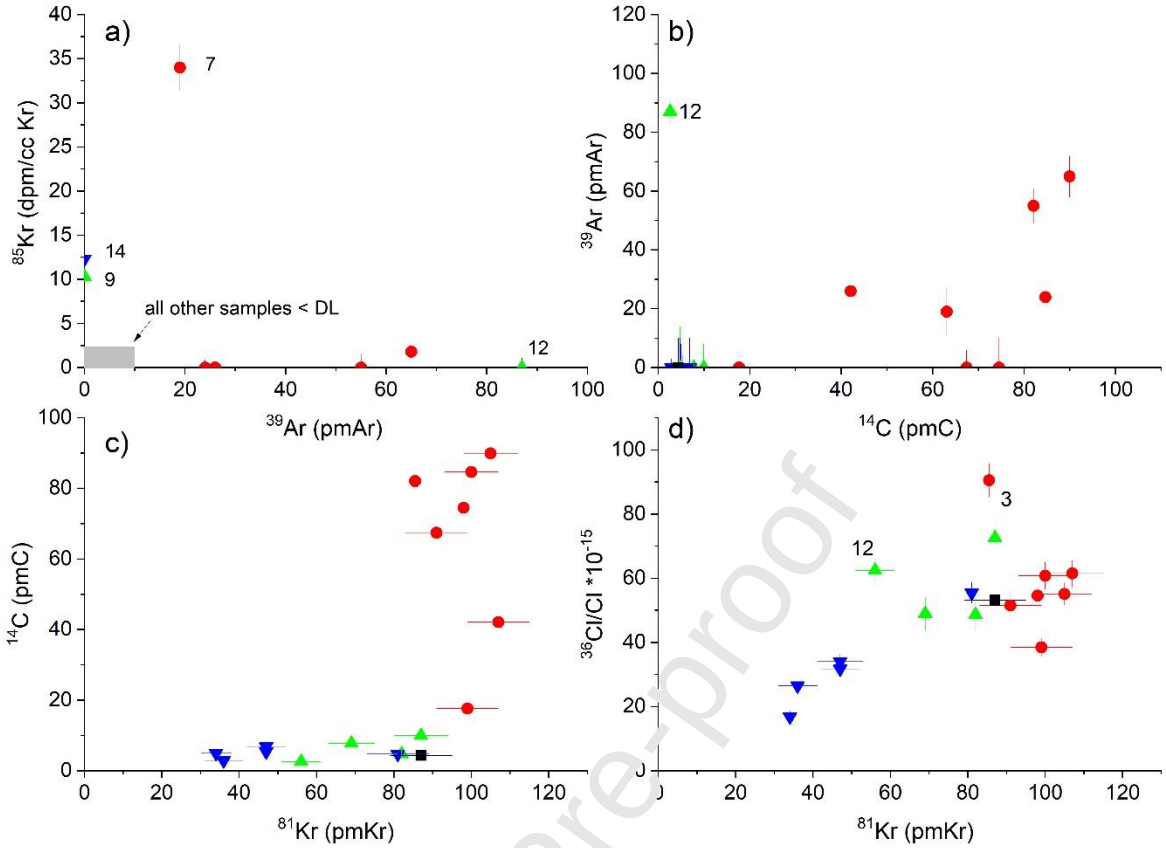


**Figure 2**: Tracer -Tracer plots showing the comparison of tracers with sequential half-lives. Red circles represent Group 1 close to the recharge zone, the green triangles represent the intermediate wells of Group 2 while the blue triangles represent the most distal wells of Group 3. The black square represents a well most likely from a more westerly recharge zone.

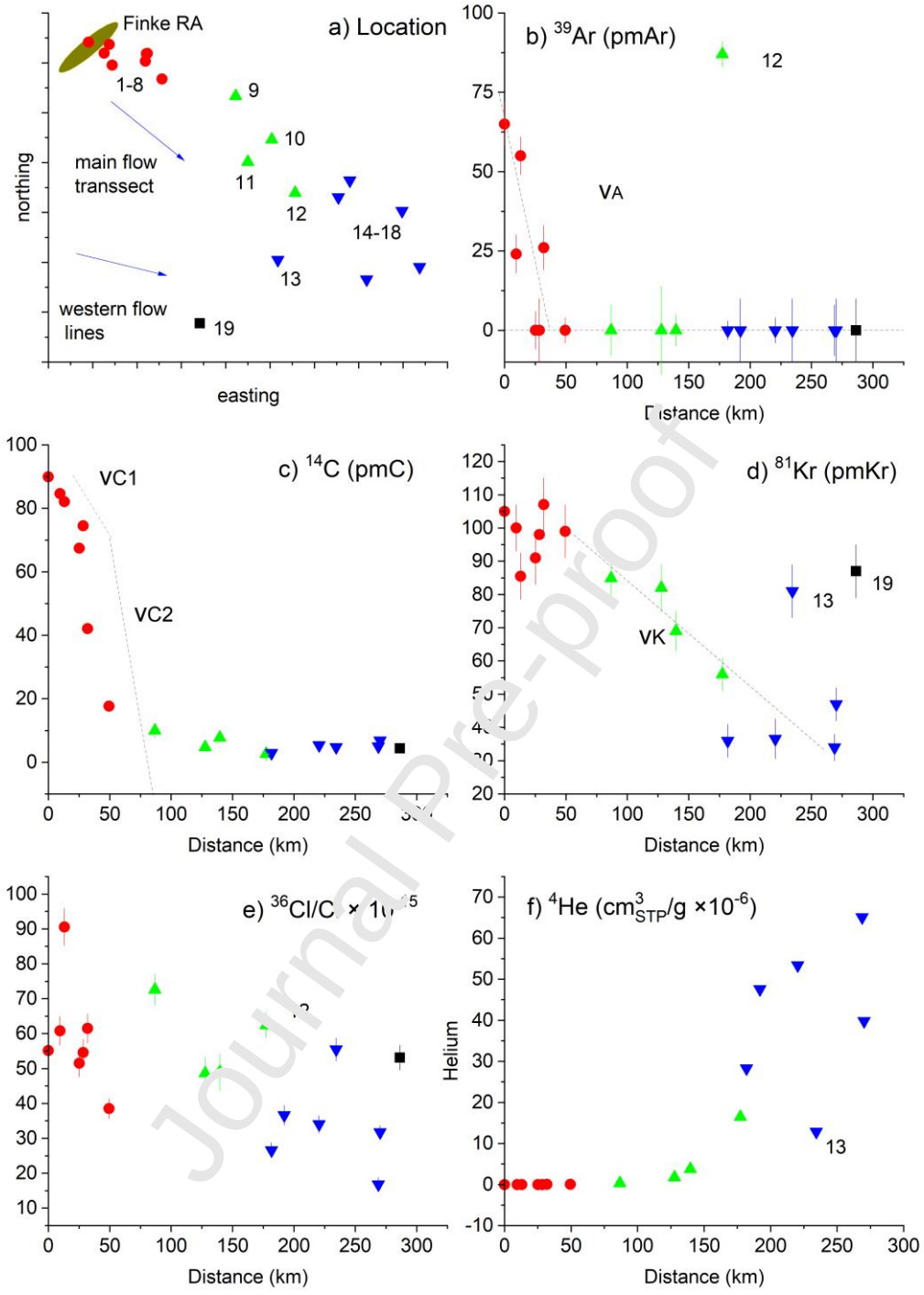


**Figure 3**: Tracer concentrations versus distance from the Finke River Recharge area (RA). The top left-hand panel shows the location of the wells as a reference. Note all the tracers show an increase in age with distance travelled along the transect.

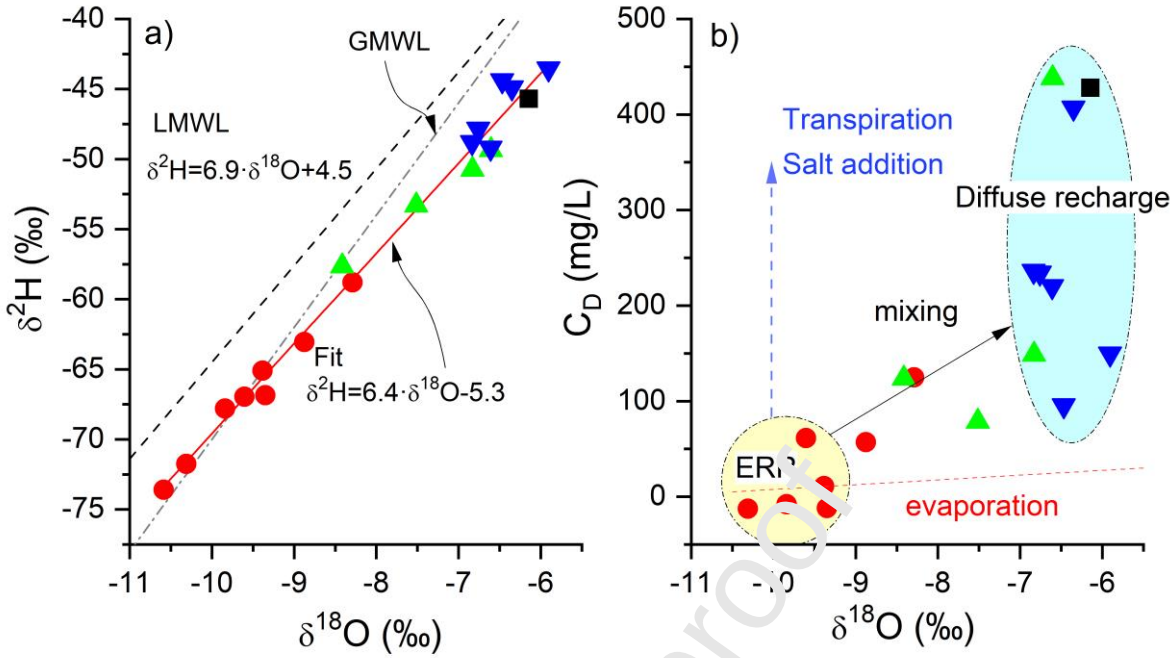


**Figure 4**: a) Plot of stable isotopic composition of the water molecule in $\delta^2H$-$\delta^{18}O$ space. The dashed-dotted line is the global meteoric water line (GMWL) $\delta^2H = 8\delta^{18}O + 10$, the dashed line represents the local meteoric water line (LMWL) $\delta^2H = 6.9\ \delta^{18}O + 4.5$ (Harrington et al., 2013), while the solid red line represents the best fit through the data. b) Displays the relationship between the $\delta^{18}O$ and the Cl concentration at recharge. The evaporation line was calculated for an equilibrium liquid-water fraction factor $\varepsilon$=1% and an initial composition of $C_{D,0}$=5 mg/L and -10.5 ‰ respectively.

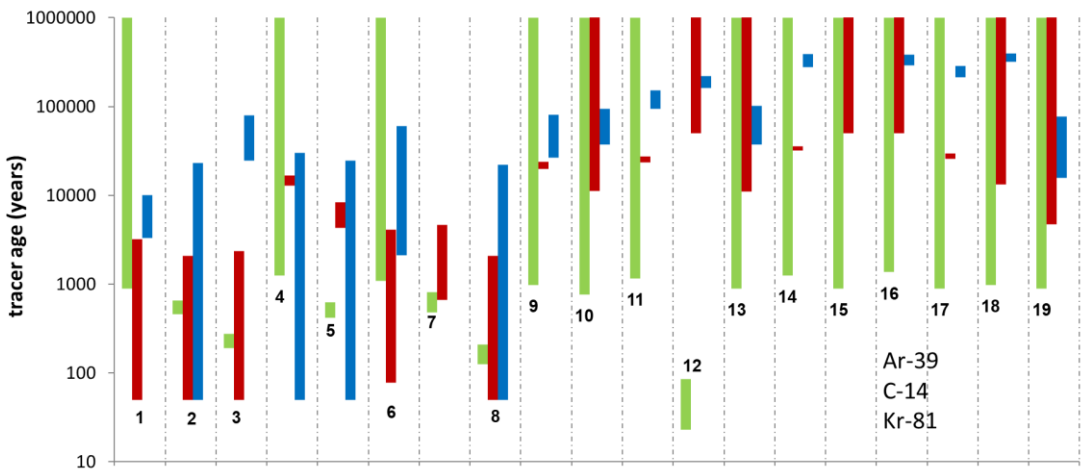


**Figure 5**: Column graph showing the comparison of possible tracer age ranges for $^{39}Ar$, $^{14}C$ and $^{81}Kr$ for the various well locations (Table 1 and 2). The length of the column represents the potential limits in the tracer's data as constrained by the measured value, the analytical uncertainty, and the half-life of the tracer. While $^{39}Ar$ is the best age constraint for the samples close to the recharge area (group 1), $^{81}Kr$ is the tracer of choice for the oldest waters. In the intermediate range (e.g., wells 4, 5) $^{14}C$ provides the best age constraint (smallest age bands).

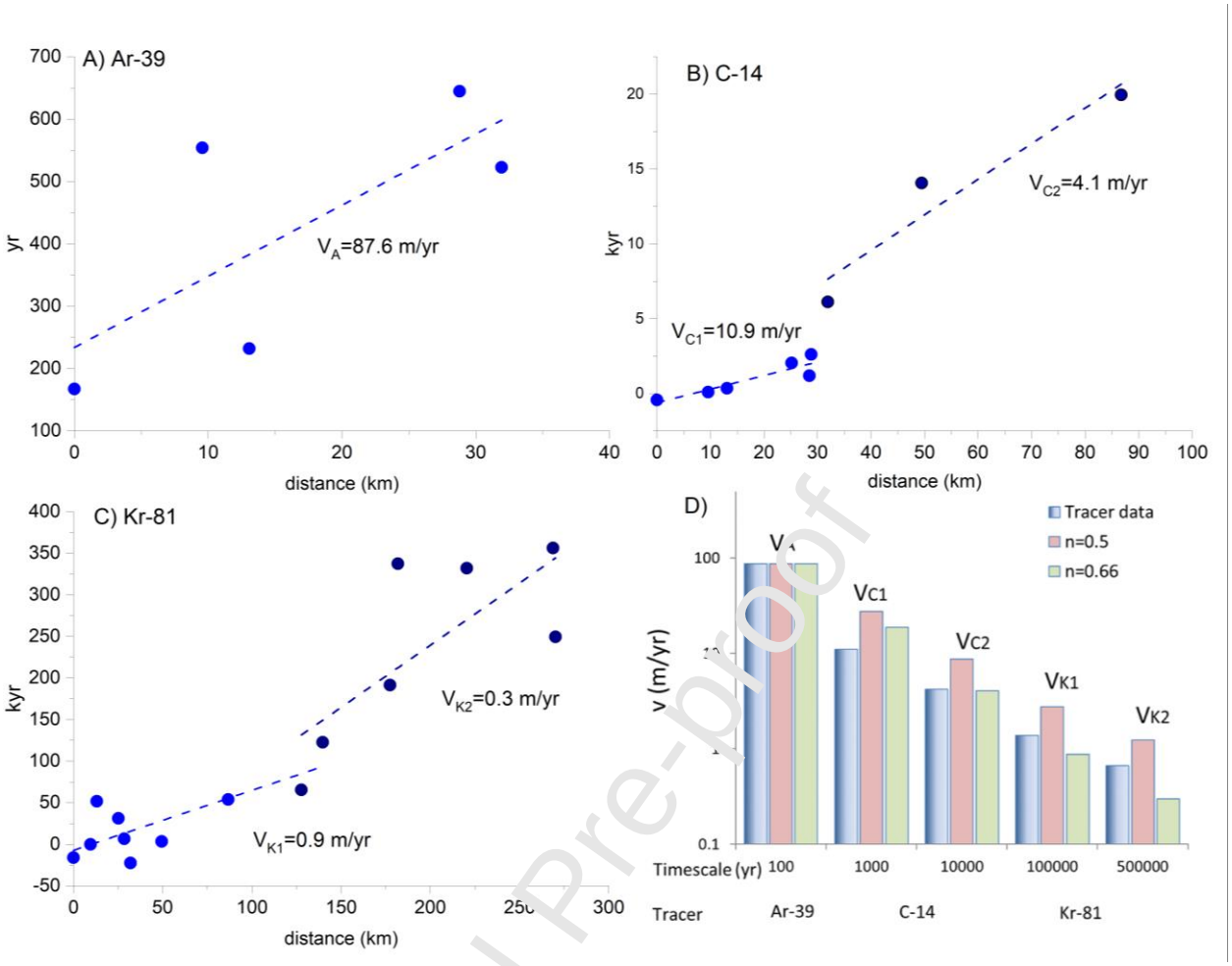


**Figure 6**: Groundwater flow velocities as function of groundwater residence times and corresponding dating tracer. Flow velocities were determined from the age gradient of the various tracers, (A) $^{39}$Ar gradient close to the recharge area, (B) $^{14}$C shows the two different velocities close to the recharge area (< 30 kms and at 30-90 kms). (C) the $^{81}$Kr data displays two different groundwater velocities. As can be observed all flow velocities decrease with increasing distance along the groundwater flow path. (D) compares the calculated flow velocity of the different tracers (blue column) versus the analytical model of a point source in an aquifer of constant (n: 0.5, red columns) or linearly increasing (n: 0.66, green columns) thickness. See Figure 6 and text for details of the model. A decent agreement between the data and the model can be observed.

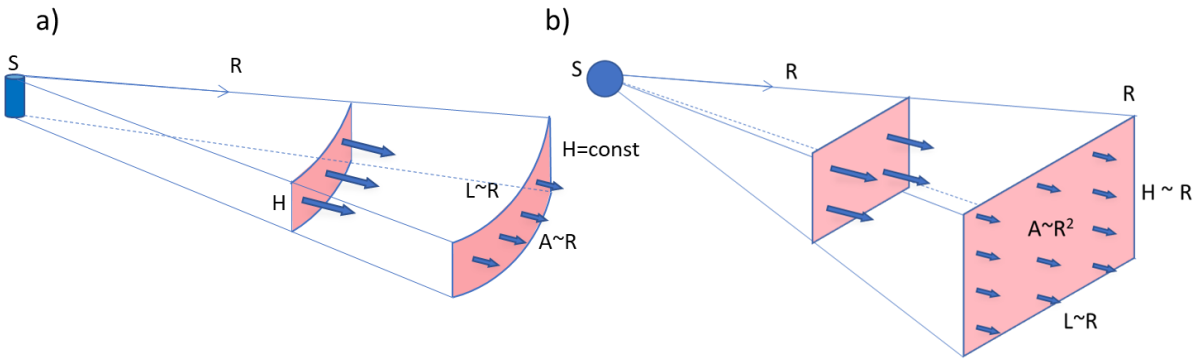


**Figure 7**: Diagrammatic representation of the analytical model of a decrease of flow velocity of groundwater originating from a point source (Eq 5). a) for constant aquifer thickness H (n=0.5 in Eq. 5) b) with linearly increasing H (n=0.66 in Eq, 5).

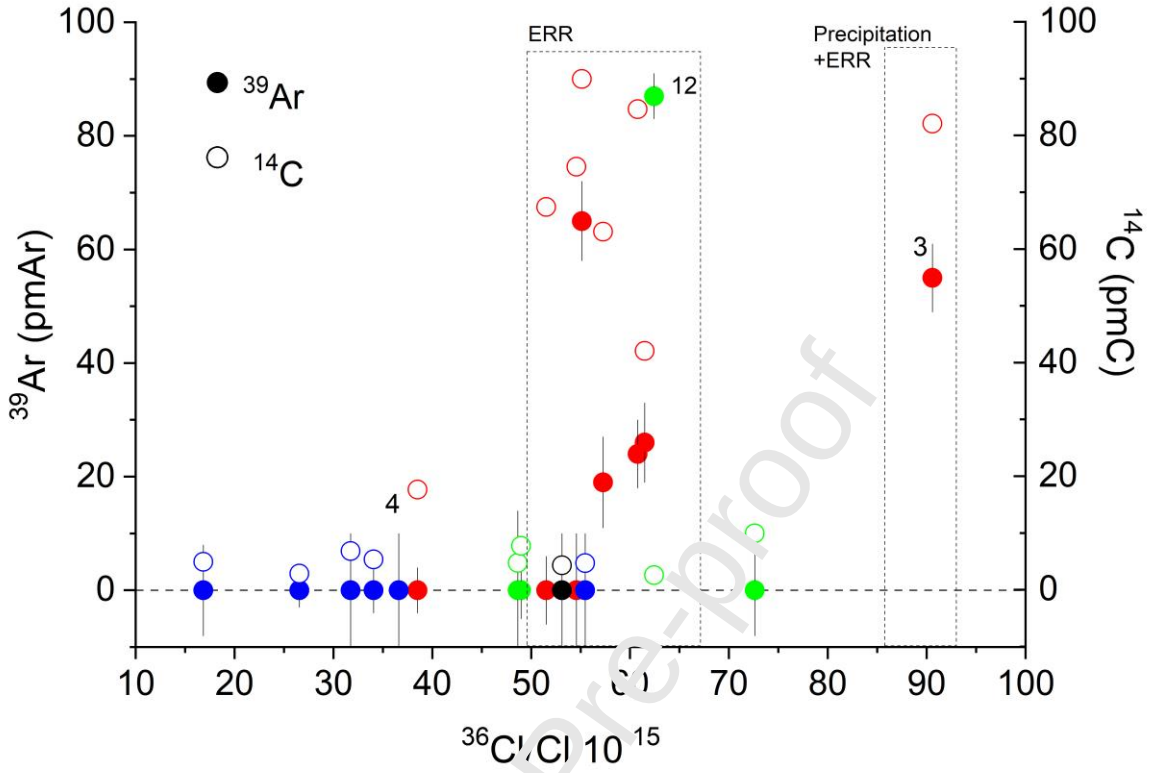


**Figure 8**: Comparison of $^{39}Ar$ (solid symbols) and $^{14}C$ activities (open symbols) versus the $^{36}Cl/Cl$ ratio. Colours indicate the different well groups as defined in Figure 1. The dashed line represents the $^{36}Cl/Cl$ input function.

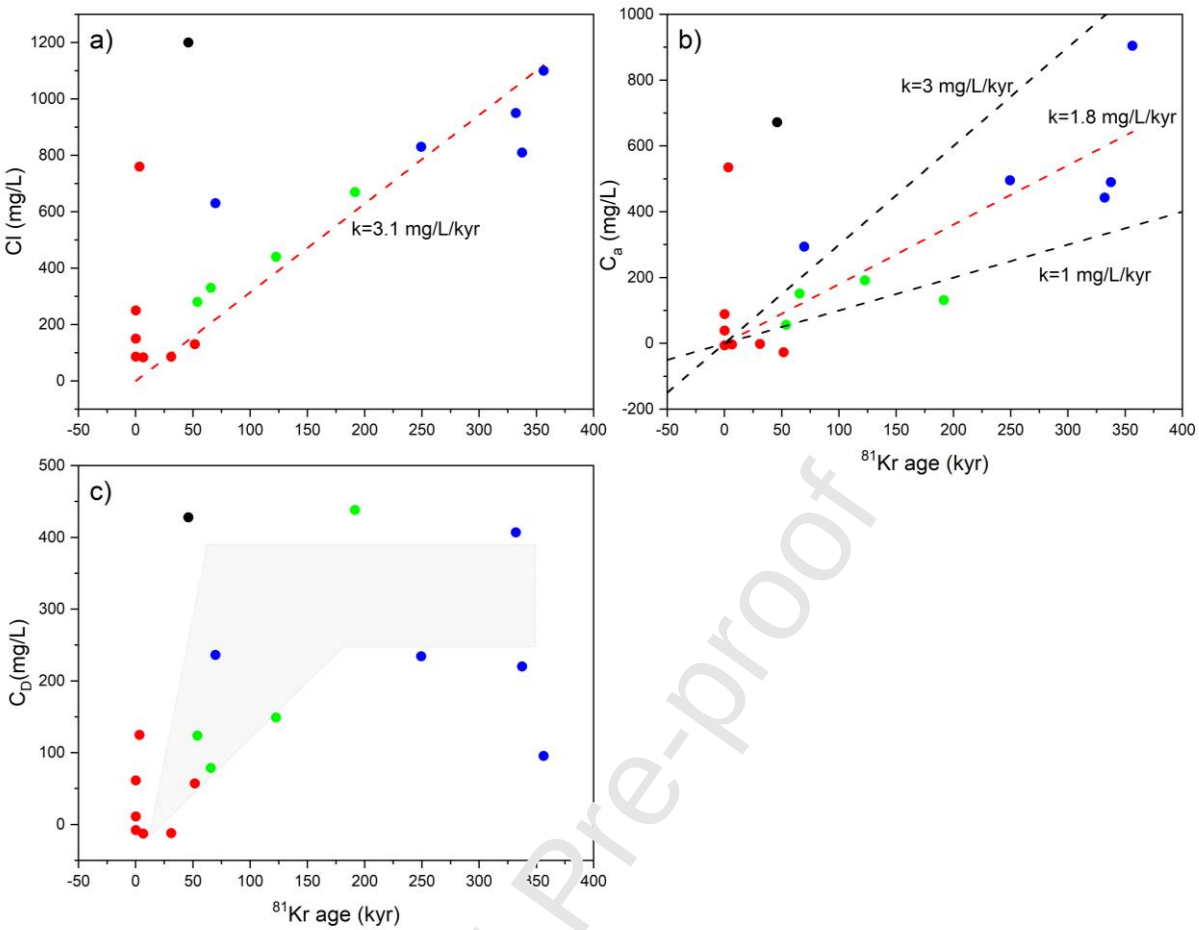


**Figure 9**: (a) Measured chloride concentration as function of $^{81}$Kr ages, (b) Calculated Cl ($C_a$) accumulated in the subsurface and (c) Calculated Cl that was already present at recharge ($C_i$) as a function of $^{81}$Kr ages. The dashed lines in a) and b) represent different Cl accumulation rates as a function of $^{81}$Kr ages.

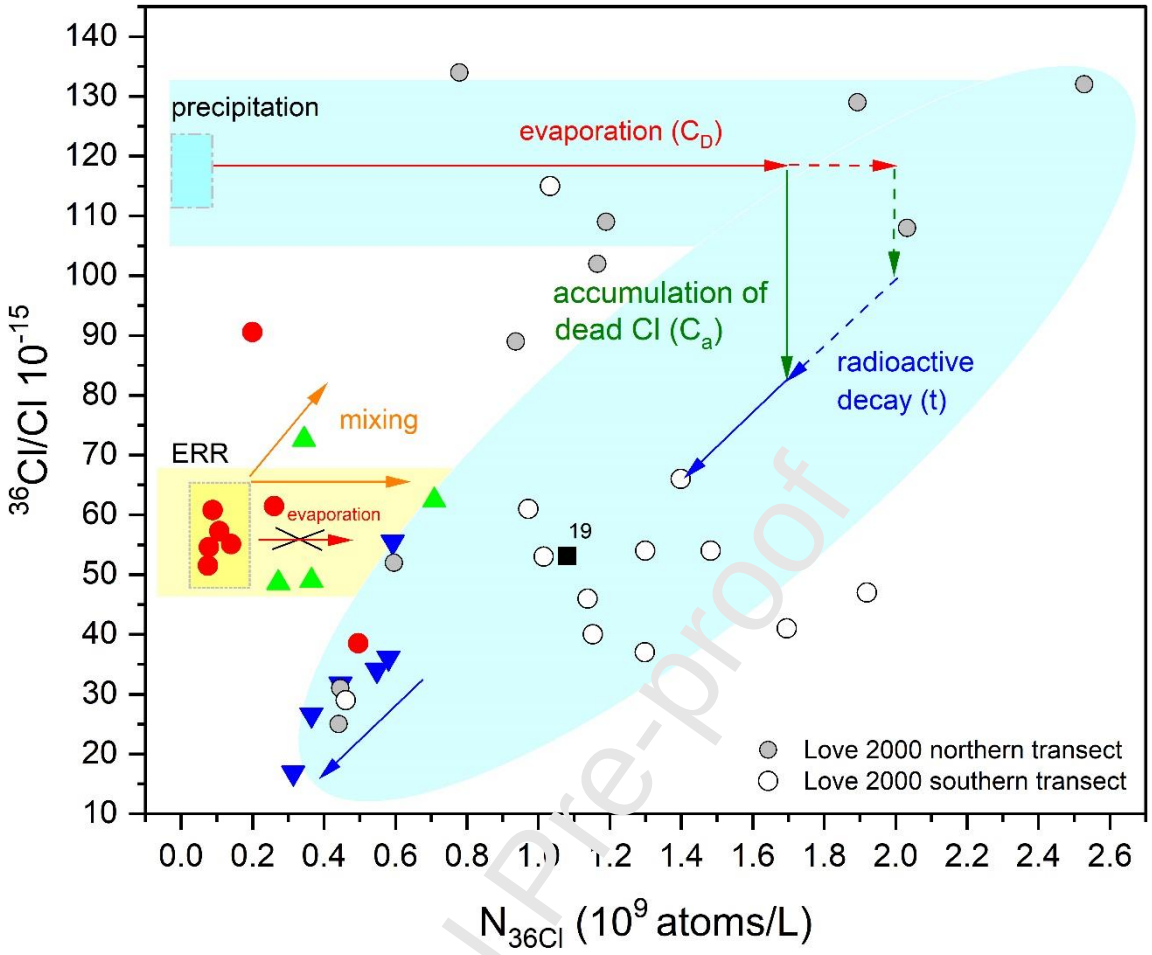


**Figure 10**: $^{36}$Cl/Cl ratios vs $^{36}$Cl concentrations ($N_{36Cl}$) in the study area. Also shown are data from Love et al 2000. The northern transect wells were sampled 500 kms to the southwest of the Finke River recharge zone while the southern transect wells were approximately 700 km to the southwest of the recharge zone. Red dots represent wells close to the recharge zone, green intermediate and blue distal samples from the recharge zone. Arrows indicate potential shifts due to different processes. Evaporative enrichment in water components originating from diffuse recharge is the only process that can significantly increase the $^{36}$Cl concentration. Accumulation of Cl from subsurface sources mainly shifts the $^{36}$Cl/Cl ratio to lower ratios but leaves the $^{36}$Cl concentration unchanged. The $^{36}$Cl/Cl signatures of group 3 waters (blue triangles) likely originate from diffuse recharge. Group 2 waters represent a mixture of ERR and diffuse recharge.

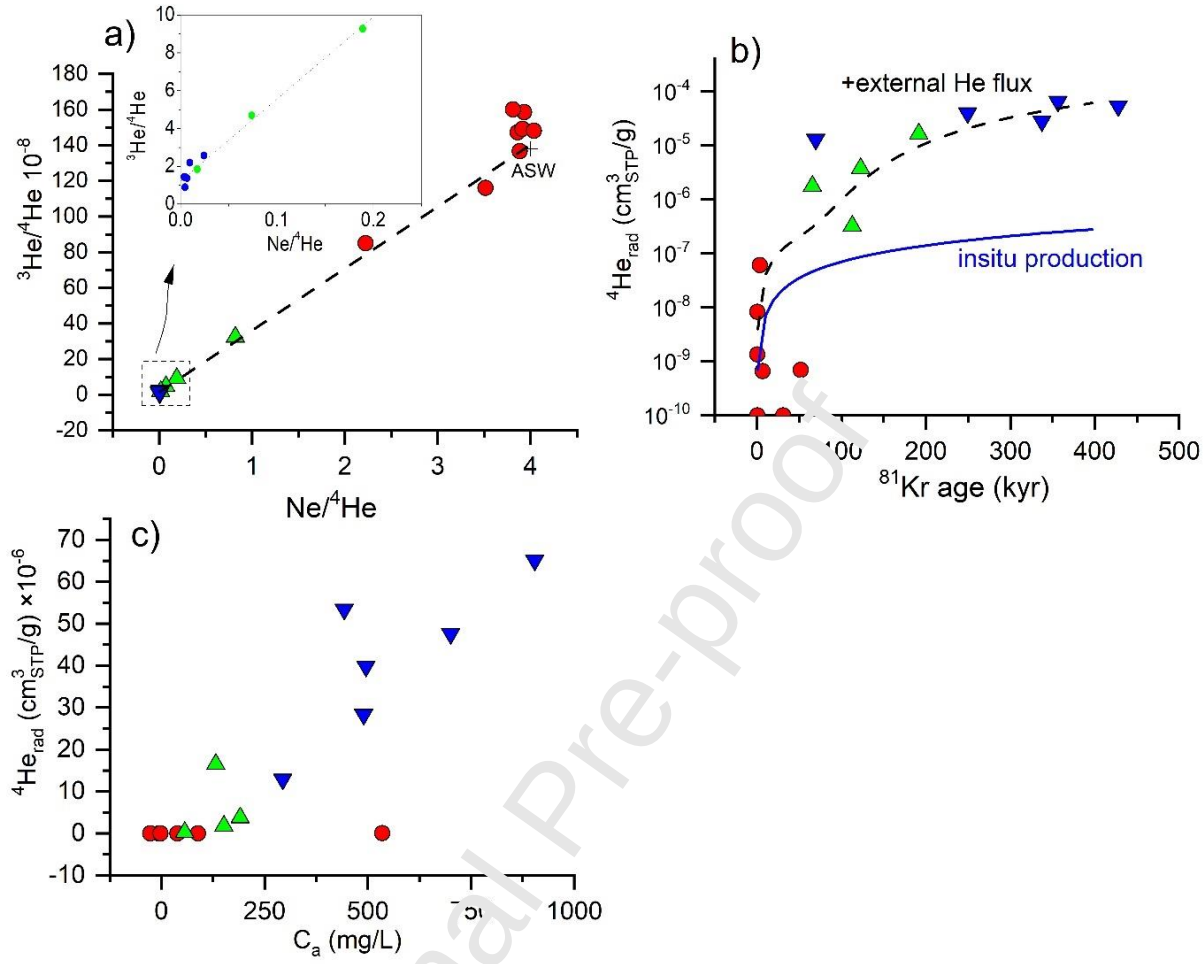


**Figure 11**: a) $^3He/^4He$ ratio versus $Ne/^4He$, ASW = air saturated water b) $^4He$ accumulation with time. The solid line shows the calculated evolutions for in-situ production only (blue) and the black dashed line represents the best fit for the model of Torgersen and Ivey (1985) (for model assumptions see text), c). Radiogenic $^4He_{rad}$ versus in the subsurface accumulated chloride $C_a$

CRediT authorship contribution statement

Roland Purtschert reports financial support was provided by Swiss National Science Foundation. Andrew Love reports financial support was provided by National Water Commission of Australia. Z._T. Lu reports financial support was provided by U.S. DOE, Office of Science, Office of Nuclear Physics.

**Declaration of interests**

☒ The authors declare that they have no known competing financial interests or personal relationships that could have appeared to influence the work reported in this paper.

**Declaration of interests**

☐The authors declare that they have no known competing financial interests or personal relationships that could have appeared to influence the work reported in this paper.

☒The authors declare the following financial interests/personal relationships which may be considered as potential competing interests:

Roland Purtschert reports financial support was provided by Swiss National Science Foundation. Andrew Love reports financial support was provided by National Water Commission of Australia. Z._T. Lu reports financial support was provided by U.S. DOE, Office of Science, Office of Nuclear Physics.

Graphical abstract

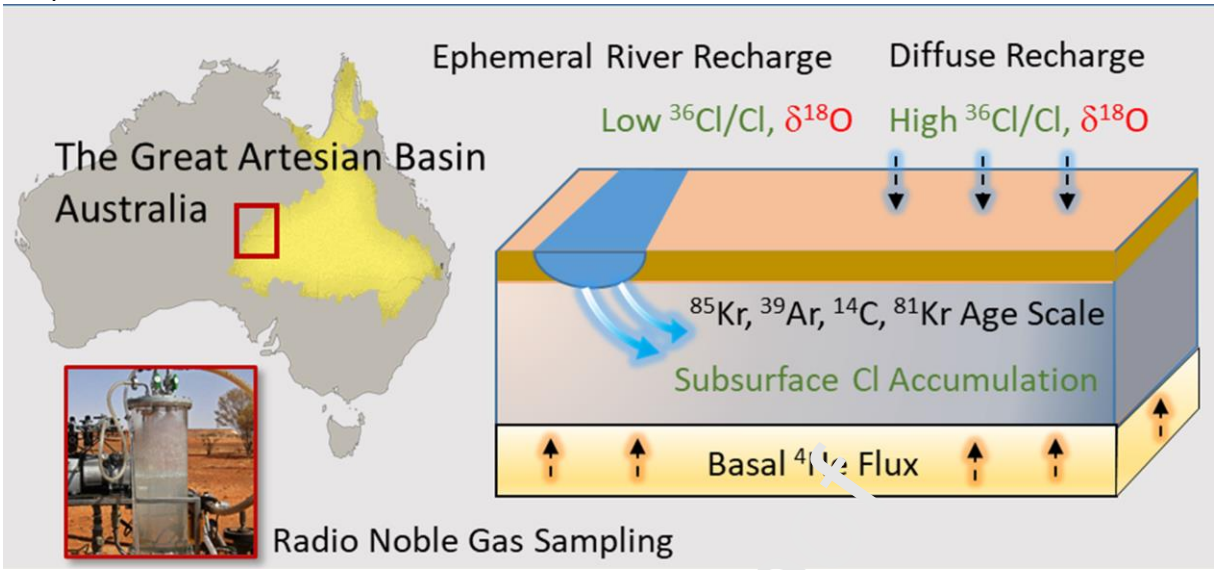

Highlights

- The first time that the whole suite of radioactive noble gas tracers $^{85}Kr$, $^{39}Ar$ $^{81}Kr$ was measured along an extended groundwater flow path
- Identification of spatial and temporal occurrence of ephemeral river recharge based on decreasing groundwater flow velocities along a flow line
- Reconstruction of changing Paleo-recharge conditions in an arid area
- Determination of critical input values for the $^{36}Cl$ and $^{4}He$ dating methods